CHEMISTRY OF MATERIALS

Article

pubs.acs.org/cm

# Probing Structure-Induced Optical Behavior in a New Class of Self-Activated Luminescent 0D/1D $CaWO_4$ Metal Oxide–CdSe Nanocrystal Composite Heterostructures

Jinkyu Han,[†] Coray McBean,[‡] Lei Wang,[‡] Jessica Hoy,[§] Cherno Jaye,[∥] Haiqing Liu,[‡] Zhuo-Qun Li,[⊥] Matthew Y. Sfeir,[§] Daniel A. Fischer,[∥] Gordon T. Taylor,[⊥] James A. Misewich,[†] and Stanislaus S. Wong*[,†,‡]

[†]Condensed Matter Physics and Materials Sciences Department, Brookhaven National Laboratory, Building 480, Upton New York 11973, United States

[‡]Department of Chemistry, State University of New York at Stony Brook, Stony Brook, New York 11794-3400, United States

[§]Center for Functional Nanomaterials, Brookhaven National Laboratory, Building 735, Upton, New York 11973, United States

[∥]Materials Science and Engineering Laboratory, National Institute of Standards and Technology, Gaithersburg, Maryland 20889, United States

[⊥]School of Marine and Atmospheric Sciences, State University of New York at Stony Brook, Stony Brook, New York 11794-5000, United States

Supporting Information

**ABSTRACT:** In this report, we synthesize and characterize the structural and optical properties of novel heterostructures composed of (i) semiconducting nanocrystalline CdSe quantum dots (QDs) coupled with (ii) both one- and zero-dimensional (1D and 0D) motifs of self-activated luminescent $CaWO_4$ metal oxides. Specifically, ∼4 nm CdSe QDs have been anchored onto (i) high-aspect ratio 1D nanowires, measuring ∼230 nm in diameter and ∼3 $\mu$m in length, as well as onto (ii) crystalline 0D nanoparticles (possessing an average diameter of ∼80 nm) of $CaWO_4$ through the mediation of 3-mercaptopropionic acid (MPA) as a connecting linker. Composite formation was confirmed by complementary electron microscopy and spectroscopy (i.e., IR and Raman) data. In terms of luminescent properties, our results show that our 1D and 0D heterostructures evince photoluminescence (PL) quenching and shortened PL lifetimes of $CaWO_4$ as compared with unbound $CaWO_4$. We propose that a photoinduced electron transfer process occurs from $CaWO_4$ to CdSe QDs, a scenario which has been confirmed by NEXAFS measurements and which highlights a decrease in the number of unoccupied orbitals in the conduction bands of CdSe QDs. By contrast, the PL signature and lifetimes of MPA-capped CdSe QDs within these heterostructures do not exhibit noticeable changes as compared with unbound MPA-capped CdSe QDs. The striking difference in optical behavior between $CaWO_4$ nanostructures and CdSe QDs within our heterostructures can be correlated with the relative positions of their conduction and valence energy band levels. In addition, the PL quenching behaviors for $CaWO_4$ within the heterostructure configuration were examined by systematically varying (i) the quantities and coverage densities of immobilized CdSe QDs as well as (ii) the intrinsic morphology (and by extension, the inherent crystallite size) of $CaWO_4$ itself.

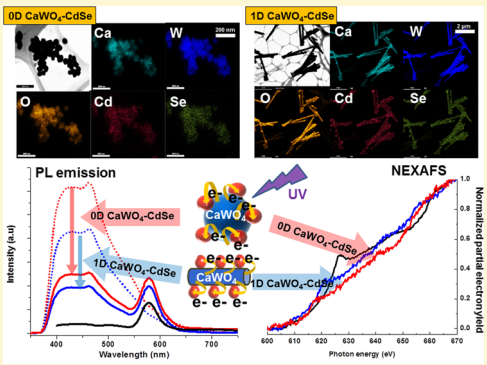


## 1. INTRODUCTION

The family of $AWO_4$ compounds (A = Ca, Ba, and Sr) has been extensively investigated both theoretically and experimentally as a result of their unique properties.[1−3] In particular, $CaWO_4$ is a material of special interest because of its intriguing and superior luminescence properties as a "self-activated" luminescent material, whose optical properties are defined to a large degree by its intrinsic structural properties.[4−6] Specifically, upon UV excitation in the spectral range of 235−260 nm, a strong blue emission near 420 nm can be observed and can be attributed to the electronic transitions associated with charge transfer between oxygen and tungsten moieties within the $[WO_4]^{2-}$ group.[2,5,7] In this light, $CaWO_4$ has been considered for potential applications including but not limited to phosphors, scintillators, optical fibers, optoelectronics, photocatalysts, and as host lattices for spin resonances.[8−12]

To date, various $CaWO_4$ possessing different morphologies, such as zero-dimensional (0D) nanocrystals as well as one-dimensional (1D) nanotubes and nanowires, have been successfully synthesized using a number of different methods,

Received: September 30, 2014
Revised: January 6, 2015
Published: January 30, 2015

ACS Publications © 2015 American Chemical Society



DOI: 10.1021/cm503611q
Chem. Mater. 2015, 27, 778−792

including sol−gel,[13] molten-salt,[14] hydrothermal,[15] electrospinning,[16] and microwave radiation protocols.[17] Recently, our group has developed a modified template technique, enabling us to prepare crystalline 1D nanostructures associated with classes of diverse materials.[18−21] Specifically, we have successfully prepared high-aspect-ratio, highly crystalline, pure $CaWO_4$ nanowires using a reasonably simple solution-based U-tube protocol.[22] Our methodology involves the use of the two arms of a glass U-tube apparatus to mediate a double-diffusion solution-based process under ambient conditions. Apart from its relative simplicity, flexibility, and generalizability, such a reaction can be run in one or two reaction steps in aqueous solvents, leading to high yields with little if any byproducts formed.

Nonetheless, it is evident that the behavior of individual nanostructures such as $CaWO_4$ can be subsequently altered and functionally tailored in unexpected ways through the formation of nanoscale heterostructures composed of different, distinctive, and complementary subunits. The key idea is that the properties of a composite aggregate whole can be favorably tuned so as to acquire more interesting and compelling attributes as compared with its individual constituent components. For example, there are numerous reports of nanoscale heterostructures incorporating tungstate compounds, such as $ZnWO_4$/BiOI, $Bi_2WO_6/TiO_2$, $CaWO_4/Bi_2WO_6$, and $SnO_2/WO_3$, which were generated with a goal toward developing novel photocatalytic and field emission properties.[23−26] Moreover, our group and others have already coupled quantum dots (QDs), which are known to be highly effective luminescent materials because of their unique size-dependent absorption properties, with either carbon nanotubes, $TiO_2$, or ZnO motifs in order to generate unique heterostructures, characterized by relevant and interesting charge transfer and transport properties for photovoltaic, photocatalytic, and light emitting diode applications.[27−34]

Most recently, QDs have been attached onto families of discrete and luminescent constituent materials including but not limited to various luminescent dyes as well as lanthanide (e.g., Eu and Tb) complexes. Examples of heterostructures created with the idea of coupling 2 or more complementary luminescent types of structures into 1 discrete whole include the formation of rare-earth doped inorganic materials, such as 0D CdSe QD-$NaYF_4$:Yb, Er[35] and CdTe QD-$YVO_4$:Eu[36] nanocrystalline constructs as well as 1D CdS QD-$LaPO_4$:$Eu^{3+}$ core−shell nanowires.[37] These specific examples highlight the community's synthetic potential to combine and ultimately transform the optical properties of two subunits within the context of engineered nanoscale heterostructures.

Nevertheless, as is apparent from the previous systems constructed, when generating novel nanoscale QD-based heterostructures incorporating either chemically distinctive or structurally unique luminescent materials, the majority of the non-QD component subunits tend to consist of rare earth (i.e., $Eu^{3+}$, $Tb^{3+}$, $Yb^{3+}$, $Sm^{3+}$, $Dy^{3+}$, and $Er^{3+}$)-activated/doped compounds. That is, the interesting optical properties of these particular materials derive primarily from the *4f*−*4f* transitions of the rare earth ion activators, which are not strongly affected by the host lattice itself and thereby give rise to comparable absorption and emission profiles, regardless of the host.[38] Therefore, the main optical characteristics of the resulting heterostructures emanate from predictable interactions between QDs and the rare earth ions.

In our group, we have sought to create more nuanced nanoscale architectures, coupling different morphological motifs in order to generate 0D−1D and 0D−3D composites in which size and morphology also play a role in determining the observed optoelectronic properties. In this vein, in terms of recent and relevant prior work, our group has reported on novel distinctive nanoscale heterostructures, comprising 0D CdSe QDs attached onto either $CePO_4$:Tb nanowires,[39] $LaPO_4$:Eu 1D nanowires, or $LaPO_4$:Eu 3D architectures.[40] In these composites, in addition to dopants, we treated structure, morphology, and chemical composition as reaction "variables" with which to tailor and control optical behavior. That is, we could selectively "toggle" between and otherwise purposely promote either energy or charge transfer processes by deliberately modulating localized chemical interactions among the constituent components of these discrete heterostructures.

Yet, to the best of our knowledge, all of the prior studies primarily rely on the use of external dopants to induce and promote interesting optical behavior within the composites. Therefore, the novelty and importance of this work is that we have created a new class of distinctive heterostructures that incorporates 1D/0D self-activating metal oxide luminescent materials (which are intrinsically luminescent by virtue of their structure) coupled with 0D QDs (possessing size-dependent luminescent properties). In so doing, we have capitalized on an untapped area of parameter space by purposely utilizing the size and morphology dependence of the inherent energy bands as a means to better characterize and manipulate our system. Specifically, we have prepared 1D $CaWO_4$ nanowire−0D CdSe QD heterostructures, wherein CdSe QDs have been successfully anchored onto the surfaces of high aspect-ratio, self-activated blue-emitting $CaWO_4$ nanowires in a process mediated with the use of a 3-mercaptoproponic acid (MPA) linking agent.

MPA represents a well-studied organic ligand that we have previously used to couple QDs with metal oxides and it consists of -SH and -COOH as terminal reactive end groups. Specifically, CdSe QDs easily and effectively adsorb SH due to the higher affinity of Cd-S, and the unbound COOH groups in MPA can be reacted with the surfaces of metal oxides through favorable electrostatic interactions.[32] In addition, we have successfully fabricated comparable 0D $CaWO_4$ nanoparticle−0D CdSe QD architectures in an analogous manner in order to compare their luminescence properties with those of our novel 1D-based heterostructures. As readily adjustable variables, we have altered both QD coverage density onto the underlying $CaWO_4$ "template" and the crystallite size of $CaWO_4$ itself.

In particular, we have characterized the optical absorption and photoluminescence (PL) emission spectra, in addition to the corresponding lifetimes of as-prepared nanoscale $CaWO_4$−CdSe QD heterostructures. In so doing, we have observed PL quenching and shortened apparent lifetimes of both 0D and 1D $CaWO_4$ in our modified, engineered heterostructures as compared with unbound $CaWO_4$. By contrast, we noted little if any significant change in the PL output and lifetimes of CdSe QDs incorporated as part of our heterostructures. Moreover, the observed PL quenching data of our 0D $CaWO_4$ nanoparticles are more pronounced as compared with analogous 1D $CaWO_4$ nanowires within our nanoscale heterostructures. We propose therefore that the "aggregate" of optical behavior, i.e., the PL quenching and the shortened PL lifetimes of $CaWO_4$ in our heterostructures, can be attributed to


DOI: 10.1021/cm503611q
*Chem. Mater.* 2015, 27, 778−792

a photoinduced charge transfer process occurring from $CaWO_4$ to CdSe QDs.

In order to support our hypothesis, we have confirmed the presence of electron transfer from $CaWO_4$ to CdSe QDs within our heterostructure motif by probing the unoccupied states of the conduction band of CdSe QDs using near edge X-ray absorption fine structure analysis (NEXAFS). X-ray absorption spectroscopy has been used as a powerful tool to examine charge transfer in various composites (i.e., $MoS_2$/carbon[41] as well as carbon nanotubes coupled with either $ZrO_2$ or $SnO_2$[42,43]) by providing information about the nature of unoccupied orbitals in the conduction band. As an example of the utility of this technique in analyzing nanoscale systems, Hamad et al.[44] have been able to observe electronic structural disorder in CdSe and InAs QDs, whereas Lee et al.[45] could probe the quantum confinement effect within CdSe QDs.

The different optical behaviors of $CaWO_4$ and CdSe QDs within our as-prepared heterostructures have been explained in the context of the inherent energy level alignments of both $CaWO_4$ and CdSe QDs. Furthermore, these particular considerations are crucial to determining not only the occurrence but also the corresponding efficiency of charge transfer between subunits in the heterostructure, which necessarily depend upon both (i) the QD coverage density onto $CaWO_4$ and (ii) the crystallite size of the $CaWO_4$ itself.

## 2. EXPERIMENTAL SECTION

**2.1. Synthesis.** *2.1.1. 1D Structures of $CaWO_4$.* A standard synthesis of 1D nanowires of $CaWO_4$ was performed, following our recently reported procedure.[46] In a typical ambient protocol, polycarbonate track-etched membranes, containing pore sizes measuring either 50 or 200 nm in diameter, were initially hydrated by immersion and sonication, and then mounted between the two half arms of a U-shaped tube. One of the two half-cells was filled with a 0.05 M $Na_2WO_4 \cdot 2\ H_2O$ solution, while the other half-cell contained a solution generated from a 0.05 M $CaCl_2 \cdot 2\ H_2O$ solution. We should note that each cell was filled simultaneously with an aqueous $Ca^{2+}$ and $WO_4^{2-}$ solution so as to obtain a chemically uniform and homogeneous $CaWO_4$ material. The aqueous solutions within the 2 half-cells of the system were then allowed to diffuse toward each other in an unperturbed manner for an incubation period of up to 24 h at room temperature.

To isolate products within the template pore channels themselves, the template membrane was gently abraded onto a smoothing stone, lubricated with mineral oil, and then sonicated for about 2 min in deionized water so as to ensure the physical removal of unwanted particles on the external surface. The rinsed template was dried in air at 70 °C before being ultimately dissolved with dichloromethane (DCM). As-prepared tungstate nanowires were later isolated from solution by washing and centrifugation steps involving DCM, followed by storage in methanol (MeOH).

*2.1.2. 0D Structures of $CaWO_4$.* Zero-dimensional (0D) $CaWO_4$ nanoparticles were prepared using a modified hydrothermal protocol from the literature.[15] Briefly, each dissolved cetyltrimethylammonium bromide (CTAB) solution, containing a mixture of 1 g of CTAB in 25 mL *n*-hexane and 1 mL of 1-pentanol, was added to two different solutions: one consisted of 260 mg of $NaWO_4 \cdot 2\ H_2O$ dissolved in 0.5 mL of deionized (DI) water, and the other comprised of 130 mg of $CaCl_2 \cdot 2\ H_2O$ dissolved in 0.5 mL of DI water so as to generate separate microemulsion solutions. Subsequently, these two microemulsion solutions were individually sonicated for 15 min, prior to mixing, and further sonicated for another 15 min. The final solution was transferred into a Teflon-lined stainless-steel autoclave (capacity of 50 mL) and sealed. The autoclave was subsequently oven heated to 140 °C for 24 h and cooled naturally to room temperature. As-prepared $CaWO_4$ nanoparticles were later isolated from solution by centrifugation upon washing with aliquots of water 7 times in order to completely remove CTAB followed by drying in air.

*2.1.3. CdSe QDs, MPA-Capped QDs, and Heterostructures of CdSe QD-1D/0D $CaWO_4$.* Colloidal CdSe QDs were prepared using a modification of an existing literature protocol.[47] Briefly, 0.2 mmol of CdO and 0.8 mmol of stearic acid were degassed at room temperature, and then heated at 150 °C under an Ar atmosphere in order to completely dissolve the precursors in a three-necked flask. Subsequently, 3.88 g each of trioctylphosphine oxide (TOPO) and hexadecylamine (HDA) were added to the flask, and the mixture was heated to 320 °C. In parallel, in an air-sensitive glovebox environment, 2 mmol of Se was dissolved in tributylphosphine (TBP) in the presence of dioctylamine (DOA). The Se solution was then injected into the hot Cd precursor solution at 320 °C, and subsequent QD growth was carried out at 270 °C for 15 s. The mixture was later allowed to cool to room temperature and was then washed with a solution of either MeOH or acetone, prior to further dissolution in hexane.

CdSe QDs capped with MPA, a mediating linker specifically chosen to connect between CdSe QDs and $CaWO_4$ in creating our heterostructures, were obtained through a ligand exchange reaction. In a typical experiment, 1 mmol of MPA ligand, dissolved in 2 mL of MeOH, was added dropwise to a suspension of as-prepared TOPO/HDA-capped CdSe QDs (0.04 mmol) in 4 mL of hexane with a molar concentration ratio of [ligands]/[QDs] = 25, with stirring. The molar ratio of [ligands]/[QDs] chosen herein is consistent with other reports for the effective promulgation of efficient ligand exchange from long alkyl chains to short thiol ligands.[48−50] Under dark conditions, individual methanolic mixtures of the MPA were stirred for 30 min. After completion of the ligand exchange process in which the CdSe QDs in the non-polar hexane layer were transferred to and subsequently dissolved into the polar MeOH layer, with the hexane layer becoming correspondingly clear (i.e., Figure S1, Supporting Information), these ligand-exchanged QDs were later collected by centrifugation and washed with both ethanol and MeOH. The resulting QDs were finally redispersed in MeOH for future use and processing. A quantitative estimate of the degree of ligand exchange efficiency can be reasonably computed by monitoring the behavior of $-CH_3$ stretching modes associated with the various ligands by means of Fourier transform infrared spectroscopy. Our data indicate a high ligand exchange efficiency of 87 ± 7%. Detailed protocols used to obtain ligand exchange efficiency values are described in the Supporting Information.

MPA-capped CdSe QDs were immobilized onto either 0D nanoparticles or 1D nanowires of $CaWO_4$ presumably through electrostatic interactions, in a manner analogous to that of previous reports of CdSe QDs attached onto various metal oxides, such as $TiO_2$ and ZnO.[34,51] For example, in a typical experiment, ∼3 mg of $CaWO_4$ in 2 mL of MeOH was added to 2 mg of MPA-capped CdSe QDs in 2 mL of MeOH. Thermogravimetric analysis (Figure S2, Supporting Information) has suggested that these MPA-capped CdSe QDs consisted of 40 wt % of MPA and 60 wt % of CdSe QDs, whereas in the resulting, as-prepared heterostructures, we noted that both $CaWO_4$ 0D nanoparticles and 1D nanowires possessed <5 wt % of molecular ligands on their outer surface. The resulting solution was then sonicated for 10 min and stirred in the dark for 2 h in order to preserve the optical integrity of the CdSe QDs. These as-prepared heterostructures were subsequently washed with MeOH to remove unbound and merely physisorbed species, and ultimately these nanomaterials were redispersed in the same solvent, prior to further study.

**2.2. Characterization.** Samples were (i) structurally characterized using a number of different complementary methodologies, including powder X-ray diffraction (XRD), thermogravimetric analysis (TGA), Fourier transform infrared spectroscopy (FTIR), Raman spectroscopy, transmission electron microscopy (TEM), energy-dispersive X-ray spectroscopy (EDS), high resolution TEM (HRTEM), and near edge X-ray absorption fine structure (NEXAFS) spectroscopy, as well as (ii) optically probed using UV−visible spectroscopy, steady-state photo-


DOI: 10.1021/cm503611q
Chem. Mater. 2015, 27, 778−792

luminescence (PL) spectroscopy, and time-resolved fluorescence lifetime spectroscopy.

*2.2.1. X-ray Diffraction.* Crystallographic and purity information on as-prepared CdSe QDs and $CaWO_4$ were initially obtained using a Rigaku Ultima III Diffractometer, operating in the Bragg configuration using Cu K$\alpha$ radiation (1.54 Å). Data were collected in a range from 15 to 70°, measured at a scanning rate of 1° per minute. To prepare as-generated QDs, 0D tungstate nanoparticles, and 1D tungstate nanowires for structural characterization, samples were rendered into slurries, i.e., in hexane for QDs and in ethanol for both 0D and 1D structures of $CaWO_4$. Samples were subsequently sonicated for about 1 min and then air-dried upon deposition onto glass slides.

*2.2.2. Electron Microscopy.* Low-magnification TEM images were obtained at an accelerating voltage of 120 kV on a JEOL JEM-1400 instrument, equipped with EDS mapping capabilities. HRTEM images coupled with complementary selected area electron diffraction (SAED) patterns were recorded using a JEOL JEM-3000F microscope equipped with a Gatan image filter (GIF) spectrometer operating at an accelerating voltage of 300 kV as well as on a JEOL 2100F analytical TEM instrument, equipped with a Gatan CCD camera, operating at an accelerating voltage of 200 kV. Specimens for all of these microscopy experiments were prepared by dispersing the as-prepared product in ethanol, sonicating for 2 min to ensure an adequate dispersion of the nanostructures, and evaporating one drop of the solution onto a 300 mesh Cu grid, coated with a lacey carbon film, for subsequent TEM and HRTEM analysis.

*2.2.3. FTIR.* FTIR spectra were collected on a Nexus 670 instrument (ThermoNicolet) equipped with a Smart Orbit diamond ATR accessory, a KBr beam splitter, and a DTGS KBr detector. As-prepared solid powder samples were placed onto the crystal surface, where data were taken with a reproducible pressure. Background correction in air was performed in the spectral range studied. FTIR data were typically recorded over the wavenumber range of 500−4000 $cm^{-1}$ spanning the far-, mid-, and near-IR regions and were subsequently evaluated in terms of expected, characteristic absorption bands. Spectra were collected using the Omnic software with a spatial resolution of 1 $cm^{-1}$.

*2.2.4. NEXAFS.* Cd $M_{2,3}$-edge and O *K*-edge NEXAFS spectra reported here were taken at the U7A NIST/DOW end station at the National Synchrotron Light Source at Brookhaven National Laboratory. The partial electron yield (PEY) signal was collected using a channeltron electron multiplier with an adjustable entrance grid bias. A variable negative bias in the range of 20−200 V was applied to reject the extraneous background due to the presence of low-energy electrons. The use of different biases allowed for both top-surface and bulk (up to 10 nm) analyses. Data were recorded in a UHV chamber at room temperature, with an incident X-ray resolution of 0.2 eV. All spectra were processed through standard pre- and postedge normalization methods. Additional experimental details can be found in previously published work.[52−55]

*2.2.5. Raman Spectroscopy.* Raman measurements using a Renishaw inVia confocal Raman microscope were performed using an experimental configuration consisting of a 100× objective lens, illuminated using either a 785 nm diode or a 514 nm Ar ion laser. The microscope was aligned by means of a computer-controlled motorized XYZ stage. Spectra were obtained at 1 $cm^{-1}$ resolution using a 1800 line/mm grating, aligned to the wavenumber region between 100−1500 $cm^{-1}$ and a 10 s exposure of the CCD detector. Data analysis of raw spectra was subsequently performed using Wire 4.0 software. Baselines were subtracted from all of the spectra presented, and individual spectra were normalized to the highest intensity of 1.

*2.2.6. TGA.* To provide for an estimate of nanoparticle concentrations, thermogravimetric analysis of the dried MPA-capped CdSe QDs as well as of 0D and 1D $CaWO_4$ nanostructures was performed using a TGA Q500 (TA Instruments) instrument. Isotherms were obtained by raising the temperature from 25 to 500 °C at a rate of 5 °C/min under a flow of ultradry high purity air, provided at a rate of 60 mL/min. The mass profiles revealed that the decomposition of the molecular ligands immobilized onto CdSe QDs as well as onto 0D and 1D $CaWO_4$ was essentially complete by 450 °C.

*2.2.7. UV−Visible and Fluorescence Spectroscopy.* Individual spectra were obtained for CdSe QDs, 0D nanoparticles of $CaWO_4$, 1D nanowires of $CaWO_4$, and associated heterostructures, all of which were individually sonicated for 2 min prior to data collection, so as to produce a homogeneous dispersion. Samples for PL spectra were dispersed in either MeOH or acetonitrile for MPA-capped CdSe QDs as well as for MPA-capped CdSe QD-$CaWO_4$ heterostructures. All of these materials were sonicated for 1 min, prior to measurement.

Extinction spectra were collected on a PerkinElmer Lambda25 instrument for samples suspended in acetonitrile, a solvent that exhibits high UV transmission. Fluorescence data were subsequently obtained at room temperature using a FluoroMax-4 spectrofluorimeter (Jobin Yvon) and an ISS PC1 photon counting spectrofluorimeter (ISS Inc., Champagne, IL) using excitation wavelengths of 260 and 460 nm, respectively. Photoluminescence intensity changes are discussed in terms of relative quenching due to the complex wavelength dependent emission features of the $CaWO_4$. The corresponding fluorescence lifetimes for CdSe QDs were measured with a FluoroMax-4 spectrofluorimeter, equipped with an IBH NanoLED, emitting at 388 nm as an excitation source, and a NanoLED controller module, Fluorohub (Jobin Yvon), operating at 1 MHz. Decay data analysis was completed using the DAS6 software (Horiba Jobin Yvon IBH). Fluorescence lifetimes for $CaWO_4$ excited at 280 nm were measured using an ISS PC1 photon counting spectrofluorimeter (ISS Inc., Champagne, IL) using frequency-domain methods. Apparent lifetimes[56] have been determined from modulation measurements ($\tau_m$) over a range of 10 kHz to 500 MHz and reported at the values where ∼50% modulation is achieved (∼50 kHz).

## 3. RESULTS AND DISCUSSION

**3.1. Structural Insights into CdSe QDs and $CaWO_4$ Nanowires/Nanoparticles.** We note that the XRD patterns of as-prepared CdSe QDs can be reliably assigned to the reflection of a crystalline hexagonal würtzite structure (JCPDS # 08-0459), as shown in Figure S3 (Supporting Information). The corresponding purity and crystallinity of (a) $CaWO_4$ nanowires, prepared by an ambient U-tube template-mediated synthesis, and of (b) $CaWO_4$ nanoparticles, synthesized by a modified hydrothermal protocol, were initially characterized using XRD. The XRD patterns suggest that the as-synthesized metal tungstate compound is composed of a single tetragonal scheelite structure with a space group of $I_{41/a}$, which agrees well with the JCPDS #72-1624 standard, as shown in Figure 1. The structure of $CaWO_4$, which represents the prototype of the scheelite incarnation of various materials such as $MgWO_4$, $CaMoO_4$, $PbMoO_4$, $PbWO_4$, $YLiF_4$, and high-pressure phases of $DyVO_4$, consists of $Ca^{2+}$ ions and $WO_4^{2-}$ groups with the corresponding coordination numbers of 8 for $Ca^{2+}$ and 4 for $W^{6+}$, as shown in Figure S4 (Supporting Information).[57,58] In addition, the constituent crystallite size, as estimated by the Debye−Scherrer formula, was found to be 37 nm for isolated 0D nanoparticles and 21 nm for individual polycrystalline samples composed of 200 and 50 nm-diameter nanowires.

The size, structure, and morphology of as-synthesized $CaWO_4$ nanowires and nanoparticles have been investigated using TEM. Typical lower and higher magnification TEM images of (i) nanowires prepared with the use of the 200 nm diameter template and of (ii) the corresponding nanoparticles are shown in Figure 2A,B and C,D, respectively. On the basis of statistical measurements of several tens of nanowires and nanoparticles pertaining to each of our samples, our as-prepared larger diameter $CaWO_4$ nanowires measure on average 230 ± 30 nm in diameter with lengths of up to 3.07 ± 1.33 $\mu$m, and the average diameters of our as-prepared


DOI: 10.1021/cm503611q
Chem. Mater. 2015, 27, 778−792

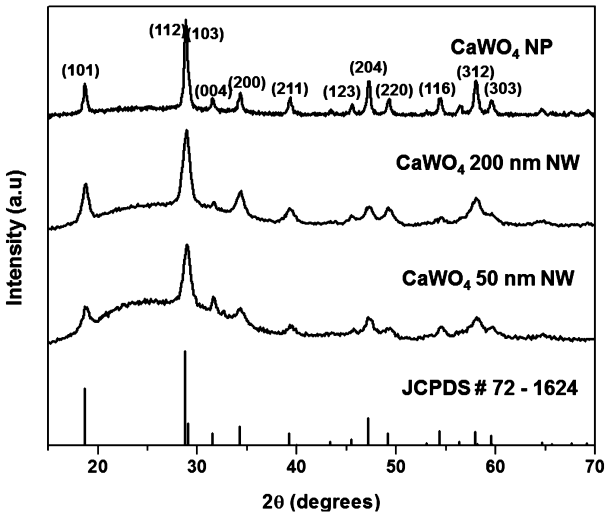


**Figure 1.** (Top to Bottom) XRD patterns of as-prepared $CaWO_4$ nanoparticles (NP) as well as of 200 and 50 nm template-derived $CaWO_4$ nanowires (NW). The corresponding JCPDS No. 72-1624 database standard for bulk $CaWO_4$ is also shown as a comparison.

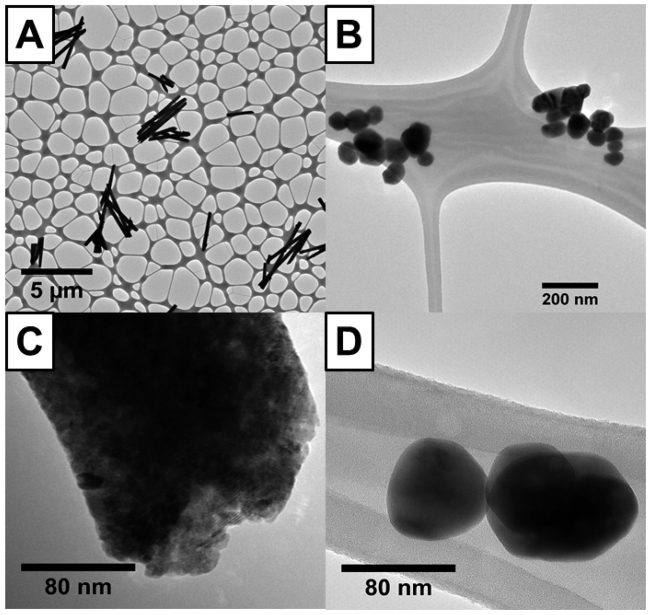


**Figure 2.** Representative TEM images at lower and higher magnifications of as-prepared $CaWO_4$ (A,C) 1D nanowires and (B,D) 0D nanoparticles, respectively.

$CaWO_4$ nanoparticles were noted to be 72.8 ± 9.0 nm. Furthermore, we have successfully synthesized $CaWO_4$ nanowires prepared with the use of smaller 50 nm diameter templates, and we found that these nanostructures possess an average diameter of 80 ± 9 nm with lengths of up to 2.16 ± 1.32 $\mu$m, as shown in Figure S5 (Supporting Information). The actual dimensions of our isolated nanowires reflect the inherent size heterogeneity of the channels associated with the commercial templates, from whence these one-dimensional nanostructures were derived.

**3.2. Structural Characterization of 1D/0D $CaWO_4$–CdSe QD Heterostructures.** *3.2.1. TEM, HRTEM, and EDS Spectra and Mapping.* Figure 3A,B and C,D highlight standard TEM and HRTEM images of $CaWO_4$ 1D nanowire-MPA-capped CdSe QD and $CaWO_4$ 0D nanoparticle-MPA-capped CdSe QD heterostructures, respectively. We were able to spatially discern distinctive regions wherein MPA-capped CdSe QDs were anchored and immobilized onto both the 0D and 1D $CaWO_4$ structures, as shown in Figure 3A and B. Moreover, the HRTEM images (Figure 3C and D) of individual MPA-capped CdSe QD–$CaWO_4$ heterostructures clearly suggest that highly crystalline CdSe QDs are indeed adjacent to and closely bound onto the outer surfaces of both $CaWO_4$ 1D nanowires and 0D nanoparticles.

In addition, HRTEM revealed interlayer spacings, corresponding to the expected lattice parameters associated with the tetragonal scheelite structure of $CaWO_4$ and with the hexagonal structure of CdSe QDs, respectively. Specifically, 0.373 and 0.476 nm were in good agreement with the expected *d* spacings for the (100) and (101) lattice planes of CdSe QDs and $CaWO_4$, respectively, within both the 1D nanowire and 0D nanoparticle-based heterostructures. The associated SAED data (insets to Figure 3C and D) revealed "less than ideal" ring patterns, which might have likely originated from the overall polycrystallinity of the structures. Particular features associated with the individual discrete diffraction patterns nevertheless could be specifically assigned either to CdSe QDs or to $CaWO_4$ nanostructures (1D and 0D), as indicated in the insets to Figure 3C and D, respectively.

From the standard TEM data, (i) the physical aggregation of QDs on the metal oxide surface and (ii) the poor differential contrast especially between the CdSe QD themselves and the external surfaces of the $CaWO_4$ nanowires and nanoparticles rendered it difficult to qualitatively and quantitatively determine the extent of coverage of QDs on the underlying 1D and 0D $CaWO_4$ templates. Hence, a detailed chemical analysis was carried out using EDS in order to more precisely probe elemental composition throughout the heterostructures, so as to confirm the presence of CdSe QDs in our composites. Specifically, representative Scanning Transmission Electron Microscopy (STEM) images of typical (a) 1D 200 nm $CaWO_4$ nanowire-based and (b) 0D $CaWO_4$ nanoparticle-based heterostructures as well as their corresponding elemental maps are highlighted in Figure 4A–F and Figure 5A–F, respectively, and these data shed light on the spatial distributions of the various constituent elements associated with both QD and metal oxide species, i.e., Ca, W, O, Cd, and Se.

Importantly, in panels E and F of Figures 4 and 5, the locations of the Cd *L*-edge and the Se *K*-edge signals overlap and coincide reasonably well with those of the Ca *K*-edge, the W *L*-edge, and the O *K*-edge signals (Figure 4 and 5B, C, and D), thereby confirming that CdSe QDs are uniformly attached onto and spatially distributed throughout the external surfaces of both $CaWO_4$ 1D nanowire and 0D nanoparticle-based architectures. In order to further confirm and corroborate the qualitative coverage density estimated by EDS mapping data (Figure S6A and B, Supporting Information), a more rigorous quantitative analysis to determine the actual coverage density of CdSe QDs on both 1D and 0D-based $CaWO_4$ structures was conducted.

In the Supporting Information, we extensively describe our detailed reasoning and the mathematical protocol used to obtain both (i) our coverage values and (ii) the efficiency of the formation of our 0D/1D-tungstate-based heterostructures, using our relatively mild synthetic approach. From the results of our analysis, the efficiency of $CaWO_4$-MPA-capped CdSe QD heterostructure formation using our synthetic protocol is


DOI: 10.1021/cm503611q
Chem. Mater. 2015, 27, 778–792

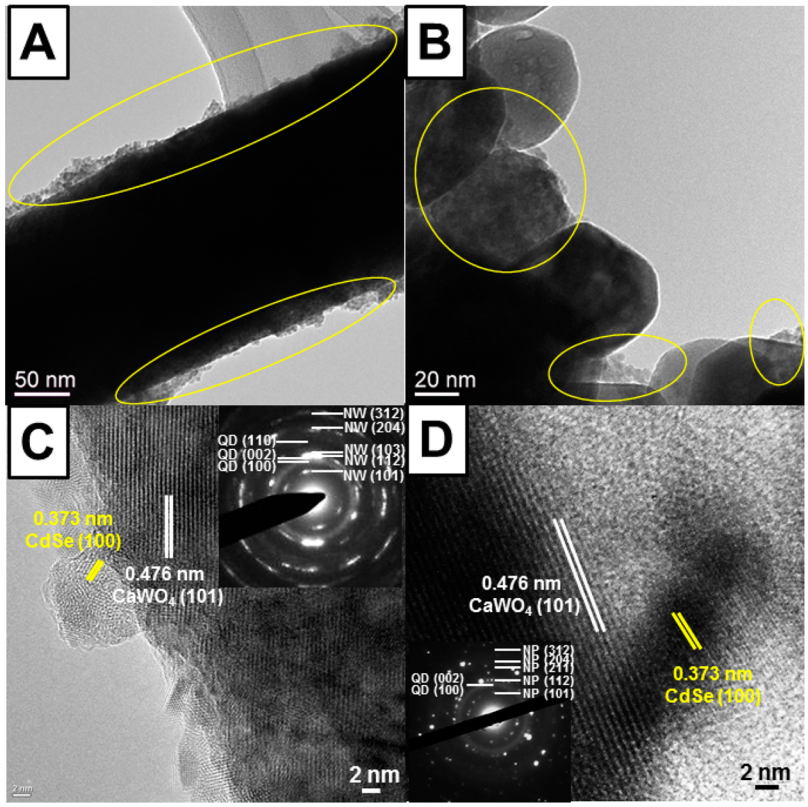


**Figure 3.** Representative (A and B) TEM and (C and D) HRTEM images and corresponding SAED patterns (insets C and D), associated with the formation of $CaWO_4$ 1D/0D-MPA-capped CdSe QD heterostructures, respectively. Yellow circles in A and B highlight regions pertaining to CdSe QDs. In C and D, "QD" designates CdSe QD reflections, whereas NW and NP denote the corresponding $CaWO_4$ 1D nanowire and 0D nanoparticle reflections, respectively.

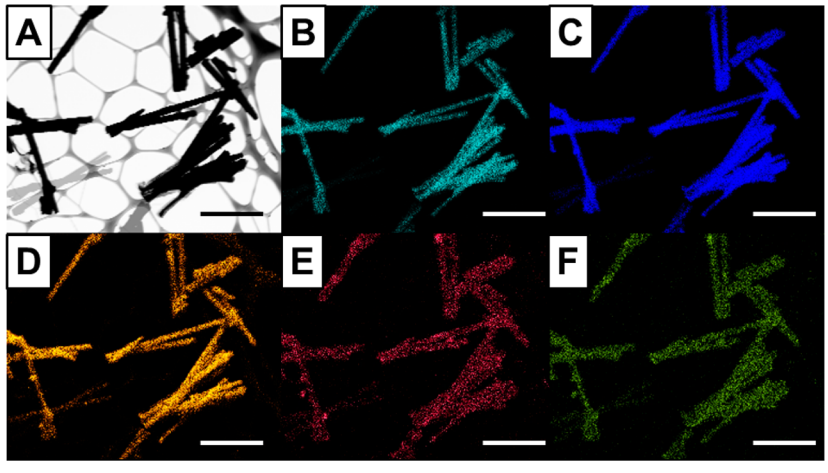


**Figure 4.** (A) Dark-field STEM image recorded on adjoining 1D $CaWO_4$-MPA-capped CdSe QD nanoscale heterostructures. (B–F) Elemental EDS mapping of the same region of nanowires, highlighting the overlapping spatial chemical distribution of Ca (bright blue), W (blue), O (dark yellow), Cd (bright red), and Se (green-yellow), respectively. The scale bar is 2 $\mu$m in every image.

~49% in the presence of 1D tungstates and ~38% when using 0D tungstates. In addition, upon normalization to identical, external, and exposed surface areas (i.e., 50 $nm^2$) of 1D and 0D structures, we calculated that approximately 17 QDs were attached onto 1D $CaWO_4$ nanowires, whereas only ~3 QDs were immobilized onto analogous 0D $CaWO_4$ nanoparticles under comparable reaction conditions, thereby suggesting that all other factors being equal, the numbers of attached CdSe QDs are slightly but perceptibly greater on the surfaces of 1D nanowire structures as compared with their 0D nanoparticulate counterparts.

*3.2.2. FTIR Analysis.* The surface chemical bonding structure of the heterostructures has been confirmed by FTIR spectra, as shown in Figure 6. Specifically, the data in Figure 6A and B highlight the FT-IR spectra of $CaWO_4$ nanowires, $CaWO_4$-MPA-capped CdSe QD heterostructures, and MPA-capped CdSe QDs, in the range of 4000–500 and 1800–600 $cm^{-1}$, respectively. The broad peak associated with the 1D $CaWO_4$ near 781 $cm^{-1}$ corresponds to the antisymmetric stretching


DOI: 10.1021/cm503611q
*Chem. Mater.* 2015, 27, 778–792

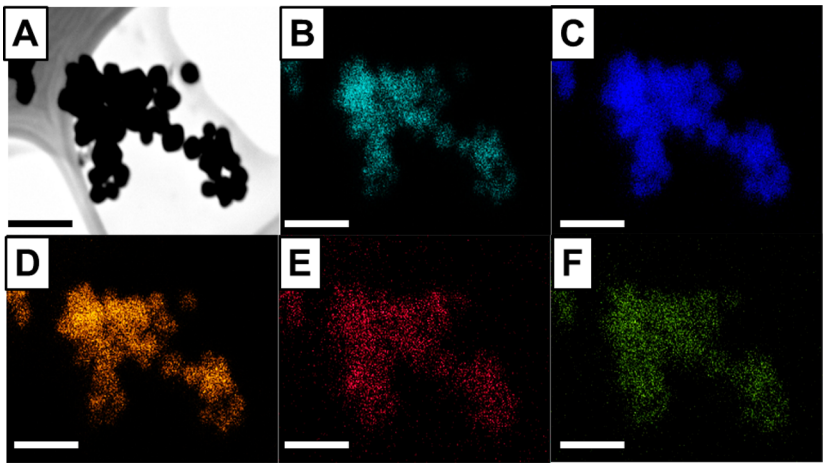


**Figure 5.** (A) Dark-field STEM image recorded on adjoining 0D $CaWO_4$-MPA-capped CdSe QD nanoscale heterostructures. (B–F) Elemental EDS mapping of the same region of nanowires, highlighting the overlapping spatial chemical distribution of Ca (bright blue), W (blue), O (dark yellow), Cd (bright red), and Se (green-yellow), respectively. The scale bar is 200 nm in every image.

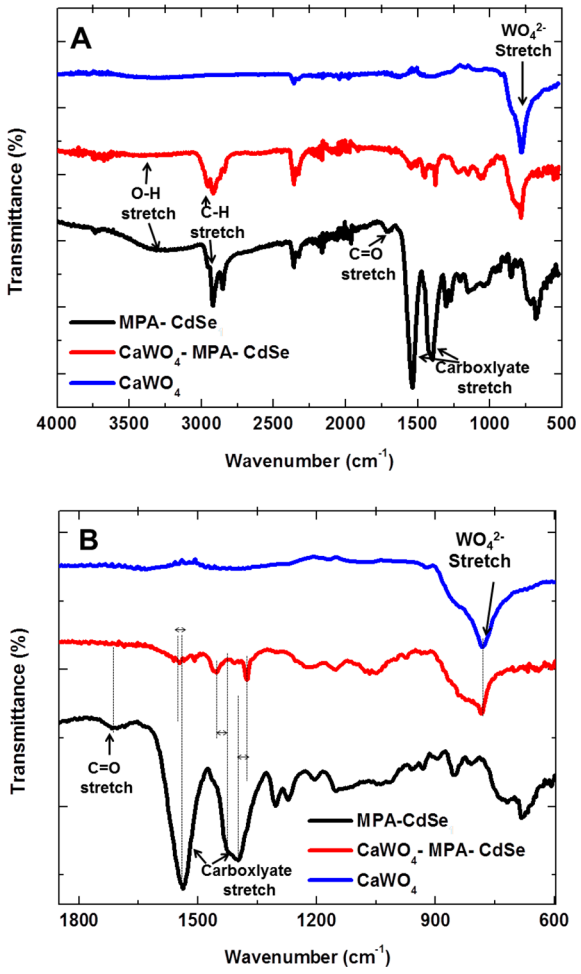


**Figure 6.** FT-IR spectra of (i) MPA-capped CdSe QDs, (ii) 1D $CaWO_4$, and (iii) 1D $CaWO_4$-MPA-capped CdSe QD heterostructures in the range of (A) 4000–500 $cm^{-1}$ and (B) 1800–500 $cm^{-1}$.

vibrational mode originating from the W–O bond configuration in $WO_4^{2-}$ tetrahedra, a finding which is consistent with other reports and with our parallel set of data on 0D $CaWO_4$, shown in Figure S7 (Supporting Information).[13,16] In effect, $AWO_4$-type scheelite oxides, possessing $S_4$ site symmetry for the A and W atoms in particular, produce the main observed absorption bands in the region of 400–1000 $cm^{-1}$.[16,59] Hence, this vibrational analysis corroborates XRD results obtained for phase-pure $CaWO_4$ nanowires and nanoparticles.

However, the presence of the bands in MPA-capped CdSe QDs, which can be ascribed to C–H stretching modes, O–H stretching vibrations, carboxyl groups, and carboxylate species, have been monitored between 2800 and 3000 $cm^{-1}$, 3340 $cm^{-1}$, 1711 $cm^{-1}$, and 1550–1390 $cm^{-1}$, respectively. We should note that the absence of a distinctive S–H peak near the region of 2400–2500 $cm^{-1}$ suggests that all "dangling" thiol moieties associated with MPA are likely to be completely bound onto the surfaces of CdSe QDs.

In the more complex $CaWO_4$-MPA-capped CdSe QD heterostructures, the IR spectra give rise to a number of specific peaks, which are invariably altered as compared with those associated with single, individual $CaWO_4$ and MPA-capped CdSe QD precursors. First, the C=O stretching vibration near 1711 $cm^{-1}$ is absent. Second, carboxylate stretching modes near 1540, 1426, and 1396 $cm^{-1}$ are shifted to 1546, 1456, and 1377 $cm^{-1}$, respectively (see Figure 6B). These data imply that the presence of either unbound $COO^-$ or COOH moieties is associated with MPA-capped CdSe QDs, which enable and facilitate attachment onto $CaWO_4$. Therefore, the formation of $CaWO_4$-MPA-capped CdSe QD nanoscale heterostructures likely follows the same mechanism previously reported to link and connect MPA-capped CdSe QDs with either $TiO_2$ or ZnO.[34,51] We should note that the position of the W–O stretching vibrational mode near 781 $cm^{-1}$ is not significantly shifted within the heterostructures themselves (i.e., Figure 6B).

*3.2.3. Raman Spectroscopic Study.* In order to more thoroughly investigate the structural variation of the $[WO_4]^{2-}$ group within $CaWO_4$ as compared with the corresponding heterostructure in more detail, we analyzed the Raman spectroscopy of both $CaWO_4$ and $CaWO_4$-MPA-capped CdSe QD heterostructures. $CaWO_4$ possessing a scheelite structure consists of isolated $[WO_4]^{2-}$ groups as tetrahedra within the crystal structure, as shown in Figure S4 (Supporting Information). Moreover, the strong covalent bonds intrinsic to the $[WO_4]^{2-}$ group can be considered as distinctive structural elemental signatures, allowing us to obtain information about the structure of the crystal lattice as well as the presence of


DOI: 10.1021/cm503611q
Chem. Mater. 2015, 27, 778–792

defects by analyzing specific variations in the Raman spectra (i.e., inhomogeneous splitting, peak shifts, and alterations in peak shapes).[60,61]

The respective Raman spectra of 1D $CaWO_4$ and of 1D $CaWO_4$-MPA-capped CdSe QD heterostructures under irradiation at 785 nm are presented in Figure 7. Several phonon

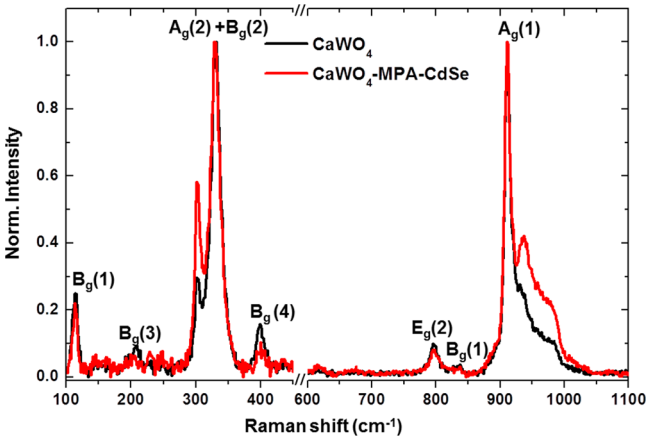


**Figure 7.** Raman spectra of 1D $CaWO_4$ and of 1D $CaWO_4$-MPA-capped CdSe 0D QD heterostructures, excited at 785 nm. Each spectrum was normalized to the highest intensity of 1.

modes within Figure 7 can be ascribed to the vibrations of W–O bonds. Specifically, there are two types of optical phonon modes within the tungstate structure: (1) internal vibrational modes, which are associated with and localized in the $[WO_4]^{2-}$ group (i.e., ~330 $cm^{-1}$ for $A_g(2) + B_g(2)$, ~400 $cm^{-1}$ for $B_g(4)$, ~796 $cm^{-1}$ for $E_g(2)$, ~839 $cm^{-1}$ for $B_g(1)$, and 910 $cm^{-1}$ for $A_g(1)$ modes) as well as (2) external vibrational modes (i.e., in the region <250 $cm^{-1}$, i.e., the $B_g(1)$ and $B_g(3)$ modes), accompanied by the deformation of the entire structure. The presence of these peaks is in accord with prior observations from previous studies of various tungstate structures.[61−64]

As shown in Figure 7, most of the peak positions and intensities associated with both 1D $CaWO_4$ nanowires and the 1D $CaWO_4$-MPA-capped CdSe QD heterostructure motifs are comparable. Moreover, we did not observe any significant variation in the line widths between the constituent $CaWO_4$ nanowires and their associated heterostructures. Specifically, the full width at half-maximum values for the $A_g(1)$ and $A_g(2) + B_g(2)$ modes for both 1D $CaWO_4$ and 1D $CaWO_4$-MPA-capped CdSe QD heterostructures are approximately 14 and 18 $cm^{-1}$, respectively. However, interestingly, the $A_g(1)$ mode (~910 $cm^{-1}$) and the $A_g(2) + B_g(2)$ combination mode (~400 $cm^{-1}$) within as-prepared $CaWO_4$-MPA-capped CdSe QD heterostructures exhibit noticeable peak splitting into 910 and 936 $cm^{-1}$ for the $A_g(1)$ band as well as 306 and 400 $cm^{-1}$ for the $A_g(2) + B_g(2)$ combination mode. The splitting of the phonon mode can potentially be attributed to a local distortion of the $[WO_4]^{2-}$ tetrahedra within the $CaWO_4$ crystals (i.e., a change in symmetry).[60]

Furthermore, the internal vibrational modes, especially $A_g(1)$ and $A_g(2) + B_g(2)$, are sensitive to the local symmetry of the tetrahedron in the crystal, and fluctuations in these vibrational modes are likely dependent on the nature of the dopants (i.e., $CaWO_4$:Nd[65]) as well as the particle size of the nanocrystals.[66] Therefore, it is plausible that the local symmetry of the $[WO_4]^{2-}$ group within the heterostructure is noticeably distorted and perceptibly perturbed when 0D CdSe QDs are anchored onto the 1D $CaWO_4$ nanowires, thereby resulting in the observed splitting and appearance of peaks located at 306 and 936 $cm^{-1}$.

Nonetheless, the overall structure of $CaWO_4$ appears not to be significantly altered since the external vibrational modes (i.e., $B_g(1)$ and $B_g(3)$) of $CaWO_4$ are located in comparable positions to those of 1D $CaWO_4$-MPA-capped CdSe QD heterostructures without any pronounced changes in the frequency ranges. This observation would presumably suggest that the inherent luminescent characteristics (i.e., the absorption and emission peaks) of $CaWO_4$ itself are not dramatically altered upon the formation of the 1D $CaWO_4$-MPA-capped CdSe QD heterostructures. We should also note that the extent of splitting of both the $A_g(1)$ and $A_g(2) + B_g(2)$ modes within unbound $CaWO_4$ is dependent upon the excitation wavelength and is dramatically reduced under visible light excitation (Figure S8, Supporting Information).

**3.3. Optical Characterization of 1D/0D $CaWO_4$–CdSe QD Heterostructures.** *3.3.1. Absorption.* Figure 8A and B display UV–visible extinction spectra of constituent 0D and 1D $CaWO_4$ nanostructures as well as of the resulting CdSe QD-

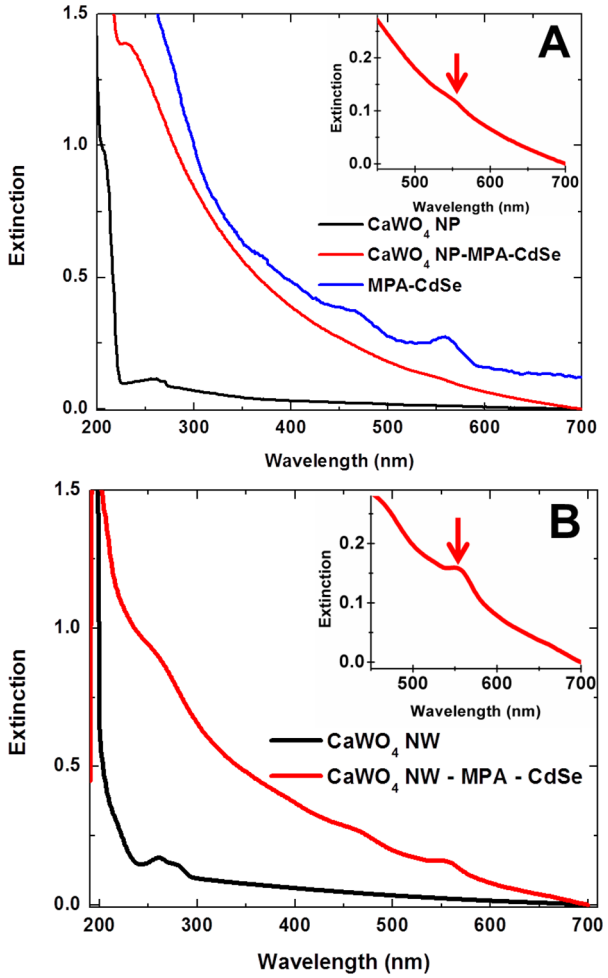


**Figure 8.** UV–visible spectra of (A) 0D $CaWO_4$ nanoparticles (NP), MPA-capped CdSe QDs, and 0D $CaWO_4$ NP-MPA-capped CdSe QD heterostructures, as well as of (B) 1D $CaWO_4$ nanowires (NW) and 1D $CaWO_4$ NW-MPA-capped CdSe QD heterostructures, respectively. The insets to A and B highlight the magnified spectral range near the absorption peak of MPA-capped CdSe QDs.



DOI: 10.1021/cm503611q
*Chem. Mater.* 2015, 27, 778–792

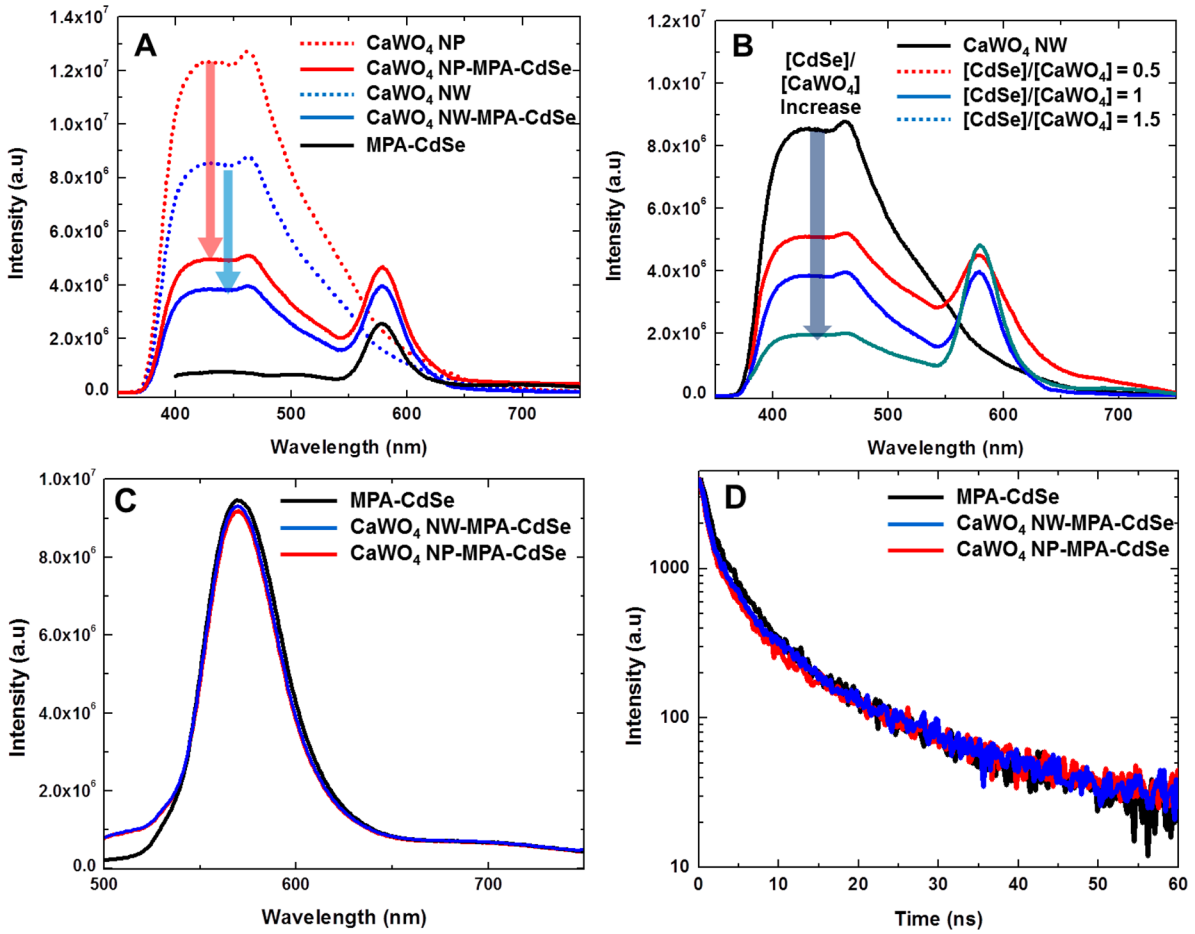


**Figure 9.** PL emission spectra of (A) $CaWO_4$ 0D nanoparticles (NP), $CaWO_4$ 1D nanowires (NW), MPA-capped CdSe QDs, 1D $CaWO_4$-MPA-capped CdSe CdSe QD heterostructures, and 0D $CaWO_4$-MPA-capped CdSe QD heterostructures, excited at 260 nm. Corresponding PL emission spectra of (B) 1D $CaWO_4$-MPA-capped CdSe QD heterostructures prepared at various concentration ratios of [CdSe QDs]/[$CaWO_4$] (namely, at 0.5, 1, and 1.5 respectively), excited at 260 nm. The 370 nm long wave path filter was used to obtain the spectra shown in A and B. PL emission spectra of (C) MPA- capped CdSe QDs, 1D $CaWO_4$-MPA-capped CdSe QD heterostructures, and 0D $CaWO_4$-MPA-capped CdSe QD heterostructures, respectively, excited at 460 nm irradiation. (D) PL decay curves ($\lambda_{ex}$ = 388 nm) associated with the excitonic emission of MPA-capped CdSe QDs, 1D $CaWO_4$-MPA-capped CdSe QD heterostructures, and 0D $CaWO_4$-MPA-capped CdSe QD heterostructures, respectively. Arrows in A and B indicate PL quenching behavior, attributed primarily to charge transfer processes occurring between $CaWO_4$ and CdSe QDs.

metal oxide heterostructures, respectively. Control samples consisting of unbound MPA-capped CdSe QDs exhibit well-pronounced absorption peaks at ~565 nm, consistent with the excitonic absorption expected for QDs of this size (Figure 8). Indeed, the UV−visible spectra of both 0D and 1D-based heterostructures suggest and reflect the presence of CdSe QDs on the $CaWO_4$ surface.

Specifically, the first exciton feature of CdSe QDs within the heterostructure is present in the extinction spectra of all of the heterostructures, appearing at ~565 nm (~2.2 eV) in MPA-capped CdSe QDs, for example (see arrows in insets to Figure 8A and B). Nevertheless, the absorbance profile of CdSe QDs within 0D versus 1D $CaWO_4$-MPA-capped CdSe QD heterostructures is less well-defined. One explanation for this observation is that the overall concentrations and therefore the corresponding coverages of particulate CdSe QDs within the final, resulting 0D $CaWO_4$-MPA-capped CdSe QD heterostructures are markedly quantitatively less than that in analogous 1D $CaWO_4$-MPA-capped CdSe heterostructures, an assertion which would be consistent with our as-obtained EDS mapping results, which have been previously shown in Figures 4, 5, and S6 (Supporting Information).

*3.3.2. Steady-State PL.* The steady-state PL spectra of 1D/0D $CaWO_4$-MPA-capped CdSe QD heterostructures are shown in Figure 9A and B. The PL spectrum exhibits a broad emission peak near 420 nm (~2.95 eV) attributable to $CaWO_4$. The characteristic broad emission band of 0D/1D $CaWO_4$ near 420 nm (~2.95 eV) can be potentially assigned to the intrinsic emission of the $CaWO_4$ structure, which is due to the presence of charge transfer between oxygen and tungsten atoms within the anion complex, $WO_4^{2-}$.[4−6] Specifically, it is well known that upon excitation from $O_{2p}$ to $W_{t2g}$, the $WO_4^{2-}$ groups effectively absorb ultraviolet irradiation within the $CaWO_4$ construct (i.e., Figure 8A, and B). In this excited state, the hole (on the oxygen) and the electron (on the tungsten) in the $WO_4^{2-}$ group are more likely to effectively form an exciton, due to their strong interactions, with the generation of a strong blue emission band near 420 nm (~2.95 eV).[4−6]

We should note that the defect-related emission attributable to typical structural defects, such as $WO_3$ Schottky defects and $Mo^{3+}$ impurities,[67−70] would normally be expected to be evident in the green−red spectral region. However, in our as-prepared 0D and 1D $CaWO_4$ nanostructures, we observed broad emission peaks near 420 nm, and in effect, the broadness


DOI: 10.1021/cm503611q
Chem. Mater. 2015, 27, 778−792

of the emission spectra of our as-prepared 1D and 0D $CaWO_4$ (i.e., fwhm ~130 nm) is comparable to what has been observed in prior reports (i.e., fwhm ~120−140 nm).[67,71] Furthermore, there is no distinctive absorption feature (Figure 8) near 673 nm, which might have been potentially attributable to an oxygen vacancy.[72] Therefore, it is much less likely that the observed emission of our 1D and 0D $CaWO_4$ herein originates from intrinsic structural defects and/or oxygen vacancies, as previously discussed. In addition, although the size of the $CaWO_4$ does not seem to induce spectral shifts,[73] both size and morphology have been shown to dictate relative emission intensities.[74] We should note that although both bare 0D and 1D $CaWO_4$ evinced differential absorption and emission behavior, especially with respect to intensities, these spectral data were actually obtained at identical sample concentrations, thereby insinuating a strong dependence on and highlighting the importance of surface quality.

Under identical excitation conditions at 260 nm (i.e., 4.78 eV), the emission intensity of the 0D/1D $CaWO_4$-MPA-capped CdSe QD heterostructures is substantially reduced as compared with that of the corresponding 1D and 0D $CaWO_4$ "building blocks" (Figure 9A). Specifically, the 0D $CaWO_4$−based heterostructures quench by a factor of 2.5, relative to bare $CaWO_4$, and the analogous 1D $CaWO_4$-based heterostructures quench by a factor of 2.2. Furthermore, in our 1D heterostructures, a reduction in the apparent lifetime from 1.3 $\mu$s for unbound $CaWO_4$ to 0.5 $\mu$s for the associated heterostructures (as determined from modulation data in frequency-domain measurements) has been observed, though the 0D heterostructures evinced less obvious changes.

Our data suggest that the PL quenching behavior of $CaWO_4$ within these QD-metal oxide heterostructures can be potentially experimentally controlled and functionally explained in light of two factors: (a) the coverage density of CdSe QDs on the underlying $CaWO_4$ template as well as (b) the intrinsic crystallite size of the $CaWO_4$ itself. First, (a) the PL quenching behavior of $CaWO_4$ appears to correlate with larger quantities of CdSe QDs bound onto $CaWO_4$. Figure 9B highlights the emission spectra collected from 1D $CaWO_4$-MPA-capped CdSe QD heterostructures, prepared using varying concentration ratios (i.e., $[CdSe]/[CaWO_4]$ = 0.5, 1, and 1.5) of CdSe QDs to 1D $CaWO_4$ and excited under 260 nm illumination. PL quenching of $CaWO_4$ is increasingly more evident in $CaWO_4$-MPA-capped CdSe QD heterostructures prepared with ever larger and increasing quantities of CdSe QDs bound onto the underlying $CaWO_4$ template. In other words, the strong $CaWO_4$ emission at 420 nm appeared to be more effectively quenched by greater numbers of CdSe QDs bound onto $CaWO_4$, i.e., with correspondingly higher concentration ratios of CdSe QDs relative to $CaWO_4$ from 0.5 to 1.5.

Second, (b) the PL quenching of $CaWO_4$ within $CaWO_4$-MPA-capped CdSe QD heterostructures was observed to be more efficient and apparent with an intrinsically larger crystallite size of $CaWO_4$. That is, we systematically analyzed the PL quenching behavior of 1D $CaWO_4$ within $CaWO_4$-MPA-capped CdSe QD heterostructures as a function of the crystallite size ($d$) of 1D $CaWO_4$. Specifically, we noted that a series of 1D $CaWO_4$ with increasing $d$ = 21, 38, and 61 nm within $CaWO_4$-MPA-capped CdSe QD heterostructures quenches by a factor of 2.2, 2.7, and 3.95 greater than that relative to bare $CaWO_4$, respectively (Figure S9, Supporting Information). Furthermore, and potentially more interestingly, the PL quenching associated with 0D $CaWO_4$ (i.e., crystallite size of ~37 nm) is far more significant as compared with that of 1D $CaWO_4$ (i.e., crystallite size of ~21 nm) within our heterostructures despite the quantitatively lower QD surface coverage (i.e., a factor of 0.18, based on EDS mapping data) on the underlying 0D $CaWO_4$ "template" as compared with the analogous 1D $CaWO_4$ framework (Figure 9A). We remark that all of these data had been normalized to the same concentration ratio of CdSe QDs to $CaWO_4$ of 1.

As discussed in section 3.2.1, we should note that the efficiency associated with heterostructure formation is ~50% and ~40% for 1D and 0D $CaWO_4$-based composites, respectively. Therefore, we expect generally greater numbers of CdSe QDs attached onto 1D $CaWO_4$ as opposed to 0D $CaWO_4$ at identical $[CdSe]/[CaWO_4]$ ratios. In addition, it is well known that the crystallite size inherently controls and is proportional to the PL quantum yield (PL QY) of luminescent materials.[75,76] Specifically, the crystallite size of 0D $CaWO_4$ ($d$ ~ 37 nm) is larger than that of 1D $CaWO_4$ ($d$ ~ 21 nm), thereby giving rise to the higher observed PL intensity of 0D $CaWO_4$ as compared with that of 1D $CaWO_4$, as shown in Figure 9A. Overall, these results indicate that though both size and coverage density represent key variables, the crystallite size is actually the more important parameter in terms of dictating the observed PL quenching behavior of $CaWO_4$ in our $CaWO_4$-MPA-capped CdSe QD heterostructures.

Furthermore, luminescent materials possessing either higher PL output or PL QY can generate a large quantity of electrons and holes upon excitation. Therefore, increasing the number of excited charge carriers has the potential for allowing for a more efficient and effective charge flow into neighboring acceptor materials, thereby resulting in a correspondingly more efficient PL quenching. This hypothesis is supported by previous reports on systems, such as QDs coupled with either ligand species, $TiO_2$, or ZnO.[77−79]

Thus, we postulate that the cumulative effects of increased PL quenching and shortened lifetimes observed for the $CaWO_4$ within the heterostructure can be mainly attributed to charge transfer emanating from $CaWO_4$ to CdSe QDs. In terms of the inherent band offsets, the energy level of the conduction band edge (CB) of $CaWO_4$ is situated above that of CdSe QDs and MPA (Figure 10), thereby resulting in potentially favorable photoinduced electron flow into the MPA-ligand-coated CdSe QDs from the metal tungstate. In order to determine the nature of the trend for $CaWO_4$ emission quenching, the quenching behaviors for both the bare and associated heterostructured moieties were studied as a function of varying (i) quantities of

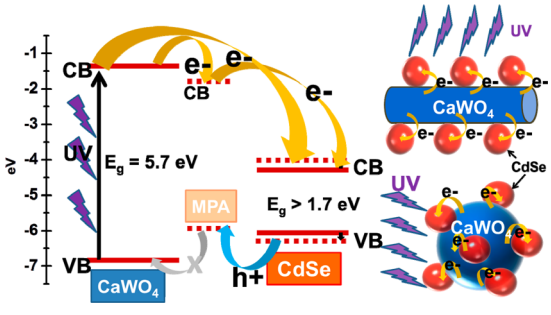


**Figure 10.** Electronic energy diagram of $CaWO_4$-MPA−capped CdSe QD heterostructures and the corresponding charge transfer schematics in these materials. $e^-$ = electron, $h^+$ = hole, $E_g$ = band gap, CB = conduction band, and VB = valence band.



DOI: 10.1021/cm503611q
*Chem. Mater.* 2015, 27, 778−792

CdSe QDs as well as (ii) the inherent $CaWO_4$ crystallite size (or morphology).

In order to examine the corresponding luminescent properties of CdSe QDs in heterostructure, the other key optically relevant species within our heterostructure, we collected PL spectra of 0D/1D $CaWO_4$-MPA-capped CdSe QD heterostructures, excited at 460 nm irradiation (Figure 9C) as well as at 260 nm irradiation (Figure 9A). By contrast with the behavior of $CaWO_4$ in our heterostructure, there was no dramatic change observed in either the CdSe QD emission peak or its PL output within the heterostructure excited at 260 nm irradiation (Figure 9A). We should note that the PL signature of CdSe QDs within the heterostructures may overlap with the emission tails of $CaWO_4$ and hence, the measured total PL intensity associated with the CdSe QD peak within the heterostructures may in fact be smaller than it appears as compared with that of unbound CdSe QDs alone.

Under 460 nm excitation, the emission profile of only CdSe QDs can be obtained; the absorption of $CaWO_4$ is negligible due to the fact that the excitation energy at 460 nm is lower than that associated with the corresponding emission profile of $CaWO_4$ ($\lambda_{em}$ = 420 nm). The PL intensity of unbound MPA-capped CdSe QDs is not noticeably altered in the profiles of CdSe QDs bound onto both 1D and 0D $CaWO_4$ structures, a finding which is also consistent with the emission profile obtained upon excitation at 380 nm irradiation (Figure S10, Supporting Information). This assertion is confirmed by the emission decay behavior, shown in Figure 9D. Specifically, the emission decay curves of unbound CdSe QDs are not significantly different as compared with that of CdSe QDs incorporated as part of $CaWO_4$-based heterostructures. In fact, the average lifetimes of unbound MPA-capped CdSe QDs and of CdSe QDs immobilized within $CaWO_4$-MPA-capped CdSe QD heterostructures are comparable ($\tau_{av}$ = 12.6 ± 0.5 ns), indicating there is no substantial evidence of charge transfer occurring from CdSe QDs to $CaWO_4$. Furthermore, we observed a similar trend with a mixture consisting of as-prepared CdSe QDs (prior to ligand exchange with MPA) physically mixed with $CaWO_4$, although the observed PL quenching of $CaWO_4$ within this sample mixture was less pronounced as compared with that noted in a chemically bound $CaWO_4$-MPA-capped CdSe QD heterostructure (Figure S11, Supporting Information).

To probe the photodegradation and photobleaching behaviors of the CdSe QDs within our $CaWO_4$-MPA-capped CdSe QD heterostructures, we analyzed their optical properties (i.e., variation in the PL emission intensity and emission peak position) under UV irradiation as a function of irradiation time (Figure S12, Supporting Information). Following prolonged UV irradiation of the $CaWO_4$-MPA-capped CdSe QD heterostructures, we were able to observe a continuous shift in the emission wavelength accompanied by an overall decrease in emission intensity of CdSe QDs. Specifically, the emission wavelength is gradually blue-shifted from 580 nm (at 0 h of illumination) to 547 nm (at 3 h of illumination). This emission wavelength blue-shift can be potentially attributed to irreversible photo-oxidation of CdSe QDs, and this type of scenario has already been discussed extensively in earlier studies.[80−82] Moreover, the PL emission intensity of CdSe QDs exponentially decreases as a function of UV irradiation time with only 36% of the initial peak intensity preserved after 3 h of exposure time. We attribute the observed photobleaching of CdSe QDs within $CaWO_4$-MPA-capped CdSe QD heterostructures to (1) the generation of nonradiative defect recombination sites during the photooxidation as well as to (2) the presence of electron transfer from the excited $CaWO_4$ into the conduction band of CdSe QDs under UV irradiation. A more detailed study of the photobleaching mechanism is beyond the scope of the current work.

We do note that it is still possible for energy transfer from $CaWO_4$ to CdSe QDs to take place under 260 nm excitation since the spectral overlap between the emission of $CaWO_4$ ($\lambda_{em}$ = 420 nm) and the absorption of MPA-capped CdSe QDs ($\lambda_{abs}$ = 400−565 nm) is not negligible. However, the energy transfer efficiency would appear to be very low since there is no distinctive difference between the emission intensity associated with unbound CdSe QDs and that of CdSe QDs bound within the heterostructure motif under 260 nm excitation (Figure 9A). To accurately determine in detail the role and behavior of photoinduced charge carriers emanating from CdSe QDs under 260 nm excitation, femtosecond transient absorption and time-resolved PL upconversion experiments will likely be needed in comprehensive future studies.

**3.4. Data Interpretation in Terms of Energy Level Alignments.** To understand all of these experimental observations, the respective energy level alignments of $CaWO_4$, MPA, and CdSe QDs need to be considered. In effect, Figure 10 shows the schematic diagram of the energy levels associated with all of these species, i.e., $CaWO_4$, MPA, and CdSe QDs. Recently, Longo et al. and others have studied and reported on the electronic level structure of bulk and nanocrystalline forms of $CaWO_4$, based on the use of both experimental techniques (TEM and HRTEM) and *ab initio* theoretical calculations.[6,83] On the basis of this work, it is reasonable to assert that the conduction band (CB) of $CaWO_4$ (i.e., −1.4 eV relative to the vacuum level) is located above the corresponding CB of MPA (i.e., ∼1.8 eV), the linking agent connecting $CaWO_4$ with CdSe QDs, as well as higher than the CB of CdSe QDs (i.e., −4.4 eV relative to the vacuum level[51]). This scenario should therefore be conducive to inducing luminescence quenching as well as a diminution of the lifetime value of $CaWO_4$ within $CaWO_4$-MPA-capped CdSe QD heterostructures as a result of electron transfer occurring from $CaWO_4$ to CdSe QDs, when the $CaWO_4$ motifs are optically excited, as shown in Figure 9A and B.

That is, it is energetically favorable for the excited electrons in the CB of $CaWO_4$ produced upon UV illumination (i.e., 260 nm) to flow into the corresponding CB of CdSe QDs in a nonradiative manner using MPA as a mediating linker, prior to the recombination of these excited electrons with the corresponding holes associated with $CaWO_4$ and the valence band (VB) of MPA. Conversely, under visible light (i.e., 460 nm) illumination, photoinduced holes generated in the CdSe QDs can readily and efficiently trap within the MPA linker, not only because of the relatively low electronegativity of thiols in MPA but also because of the correspondingly higher VB level of MPA (e.g., −5.5 eV[84]) as compared with that of CdSe QDs (e.g., −6.1 eV). However, the photoinduced holes are not likely to flow into $CaWO_4$ due to the noticeably lower VB of $CaWO_4$ (e.g., −7.1 eV), thereby resulting in little if any reduction of the PL signal in CdSe QDs incorporated within heterostructure motifs, which is consistent with what we in fact observed.

**3.5. Confirmation with NEXAFS Measurements.** In order to further confirm the presence of electron transfer from $CaWO_4$ to MPA-capped CdSe QDs and thereby explain the PL quenching and shortened lifetimes of $CaWO_4$ within the


DOI: 10.1021/cm503611q
Chem. Mater. 2015, 27, 778−792

heterostructure, we acquired the NEXAFS spectra of 1D $CaWO_4$-MPA-capped 0D CdSe QD heterostructures as well as of MPA-capped CdSe QDs. Specifically, the NEXAFS spectra associated with the Cd $M_{2,3}$ edge of the 1D $CaWO_4$-MPA-capped 0D CdSe QD heterostructures and with MPA-capped 0D CdSe QDs are shown in Figure 11A. The Cd $M_{2,3}$ edges can

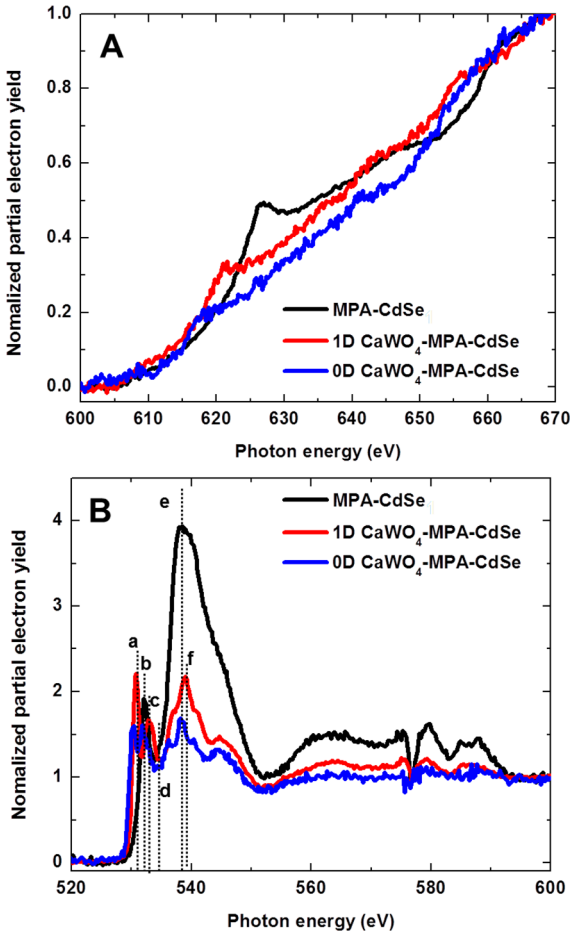


**Figure 11.** (A) Cd $M_{2,3}$ edge and (B) O *K*-edge partial electron yield spectra of both 1D/0D $CaWO_4$-MPA-capped CdSe 0D QD heterostructures as well as of MPA-capped CdSe QDs. All of the spectra have been pre- and postedge normalized.

be used to probe the bottom of the CB in CdSe QDs since both theory and calculation suggest that the bottom of the CB is predominantly composed of the Cd 5s state. Indeed, the Cd $M_{2,3}$ edges provide insight into the transition between the initial 3p state and the unoccupied 5s states, which follows typical dipole transition selection rules.[45]

Interestingly, the PEY intensity of 1D $CaWO_4$-MPA-capped CdSe 0D QD heterostructures in acquired Cd $M_{2,3}$ edge spectral data is noticeably reduced, and the peak itself is shifted to lower photon energy as compared with that of MPA-capped CdSe QDs alone. Importantly, the PEY intensity is proportional to the unoccupied electronic density of states.[85−87] Hence, the reduction in the number of unoccupied states associated with the CB in MPA-capped CdSe QDs within $CaWO_4$-MPA-capped CdSe QD heterostructures as compared with the corresponding conduction band of unbound MPA-capped CdSe QDs (Figure 11A) is suggestive of an increase in the number of electrons in the Cd 5s states (the CB of CdSe QDs) within the heterostructure, thereby providing for direct evidence of electron transfer occurring from $CaWO_4$ to CdSe QDs. Furthermore, a peak shift to lower photon energy within the heterostructure confirms that the position of the CB associated with the CdSe QDs suggests that CdSe is acting as an electron acceptor.

In general, the nature of the peak shift depends on the local chemical and electronic environment of the unpaired electron. A shift to higher binding energy likely signals the donation of electrons, whereas a shift to lower energy is more indicative of electron acceptor behavior.[86,88,89] We should note that the reduction of the PEY intensity accompanied by a peak shift of MPA-capped CdSe QDs within the 0D $CaWO_4$-MPA-capped CdSe 0D QD heterostructures is more pronounced than the analogous effects associated with 1D $CaWO_4$-based heterostructures. This overall observation implies that electron transfer from 0D $CaWO_4$ to MPA-capped 0D CdSe QDs is likely to be more efficient than that between the corresponding 1D $CaWO_4$ and 0D CdSe QDs, an assertion which is consistent with the optical PL data previously shown in Figure 9A.

O *K*-edge NEXAFS spectra (Figure 11B) additionally support the idea of electron transfer from $CaWO_4$ to MPA-capped CdSe QDs. Specifically, peaks b (532.1 eV) and e (538.1 eV) correspond to the transition from the oxygen 1s to the $\pi^*$ state of C═O and the $\sigma^*$ state of C−O, respectively, with the peak intensity itself proportional to the unoccupied electronic density of states associated with the MPA ligands,[85−87] consisting of SH (bound to CdSe) and of COOH (bound to $CaWO_4$) species. We find that the intensities of peaks b and e are significantly reduced when the MPA ligands capped onto CdSe QDs are anchored onto $CaWO_4$ and that these intensities are further reduced for 0D $CaWO_4$-based heterostructures. Thus, we can infer that (a) MPA is likely acting as an electron acceptor within the heterostructure configuration, an idea consistent with the picture presented in Figure 10, and that (b) electron transfer from 0D $CaWO_4$ to MPA is likely to be more efficient than the corresponding process from 1D $CaWO_4$ to MPA.

We should note that the absence of the OH peak (i.e., peak d, 534.9 eV) within the heterostructure reveals that COOH groups were likely replaced by carboxylate groups due to the chemical generation of the heterostructure through the adsorption of COOH groups onto $CaWO_4$, an assertion which is consistent with the FT-IR spectra (Figure 6). Furthermore, peaks a (i.e., 530.7 eV for 1D and 530.2 eV for 0D), c (i.e., 533.0 eV for 1D and 531.8 eV for 0D), and f (i.e., 538.9 eV for 1D and 538.3 eV for 0D) can be assigned to transitions associated with 1s−$e^*$ and 1s−$t_2^*$ for W−O and 1s−3d for Ca−O, respectively, pertaining to $CaWO_4$. It is known that the O 2p states within W−O bond mainly affect the behavior of the valence band of $CaWO_4$, as is apparent from complementary measurements and calculations.[90−92]

Hence, based on all of our data, it is reasonable to postulate that the PL quenching behavior coupled with the reduction in lifetimes of 1D/0D $CaWO_4$ within 1D/0D $CaWO_4$-MPA-capped CdSe QD heterostructured composites can be viewed collectively as a consequence of electron transfer from $CaWO_4$ to CdSe QDs. It is still possible that energy transfer contributes to some extent by directly quenching a fraction of the photogenerated carriers within $CaWO_4$. However, in order to determine its precise role and, moreover, to quantify the relative contributions of charge versus energy transfer between $CaWO_4$ and CdSe QDs in the overall observed optical behavior, femtosecond transient absorption and time-resolved


DOI: 10.1021/cm503611q
Chem. Mater. 2015, 27, 778−792

PL upconversion experiments will likely be needed in future studies.

## 4. CONCLUSIONS

Preformed CdSe semiconducting 0D nanocrystals ($d \sim 4$ nm) have been successfully attached onto self-activated luminescent $CaWO_4$ metal oxide (i) 1D nanowires, possessing very high-aspect ratios (i.e., ~230 nm in diameter and ~3 $\mu$m in length) and (ii) 0D nanoparticles ($d \sim 73$ nm) by means of electrostatic interaction between the ligands (MPA) bound to the CdSe QDs and the external surfaces of 1D/0D $CaWO_4$ structures. In so doing, we have created a new class of heterostructures by taking advantage of and functionally combining two distinctive types of materials, whose intrinsically interesting individual optical behaviors primarily derive from their inherent structure, i.e., 0D QDs coupled with luminescent metal oxide tungstates. That is, by contrast with much of the prior literature, we are not relying on using dopants but rather on precisely tuning structural nuances of the constituent nanoscale components themselves to generate the ensuing novel optical characteristics of our resulting nanomaterials.

From a photophysical perspective, the resulting nanoscale 1D and 0D $CaWO_4$-MPA-capped CdSe QD heterostructures were found to display PL quenching and shortened lifetimes of 0D/1D $CaWO_4$ as compared with unbound $CaWO_4$, due to photoexcited charge transfer occurring from $CaWO_4$ to CdSe QDs. This assertion has been confirmed using NEXAFS measurements as manifested in both (i) a reduction in the intensity of PEY at the conduction band of CdSe QDs along with (ii) a peak shift to lower photon energy, as compared with unbound QDs, based on studies of our heterostructure motifs. Conversely, there was no significant difference in the PL outputs and lifetimes of CdSe QDs incorporated within our as-prepared heterostructures as compared with unbound CdSe QDs.

This noticeable difference in optical behavior between $CaWO_4$ and CdSe QDs can be explained by the relative energy level alignment between $CaWO_4$ and CdSe QDs. Specifically, the CB of $CaWO_4$ is situated significantly higher than that of the corresponding CB levels of the MPA linker and that of CdSe QDs, thereby resulting in favorable electron transfer from $CaWO_4$ to CdSe QDs through the intermediary MPA agent. However, the VB of MPA-capped CdSe QDs is located noticeably above that of $CaWO_4$, which is not necessarily ideal for photoinduced charge transfer from CdSe QDs to $CaWO_4$.

Furthermore, PL quenching of $CaWO_4$ within our as-produced heterostructures is more pronounced and directly correlated with increasing amounts of CdSe QDs and with the larger intrinsic crystallite size, associated with a higher PL QY, of $CaWO_4$. Interestingly though, the observed PL quenching of 0D $CaWO_4$ is greater than that of 1D $CaWO_4$ within as-synthesized $CaWO_4$-MPA-capped CdSe QD heterostructures, despite the slightly lower coverage and quantity of CdSe QDs attached and bound onto the underlying 0D versus 1D $CaWO_4$ templates. We ascribe such unexpected behavior mainly to the higher PL output and PL QY associated with the larger crystallite size of 0D $CaWO_4$, which in turn generates more photoinduced charge carriers, thereby resulting in greater PL quenching as compared with the 1D $CaWO_4$ motif.

Overall, we propose that understanding and clearly delineating charge and energy transfer processes in our model $CaWO_4$–CdSe QD heterostructures are fundamentally important for understanding the optoelectronic behavior of nanomaterial interfaces. Moreover, the implication of our studies is that we can enable not only the potential to design new types of photocatalytic architectures under various irradiation conditions but also the ability to tune the optoelectronic properties of nanomaterials for possible incorporation into functional nanoscale devices.

## ■ ASSOCIATED CONTENT

### Supporting Information

Additional structural characterization (including microscopy and spectroscopy) results, detailed calculations, and lifetime data. This material is available free of charge via the Internet at http://pubs.acs.org.

## ■ AUTHOR INFORMATION

### Corresponding Author

*E-mail: sswong@bnl.gov; stanislaus.wong@stonybrook.edu.

### Notes

The authors declare no competing financial interest.

## ■ ACKNOWLEDGMENTS

This research (including support for J.K.H, C.M, L.W, J.H., H. L, M.Y.S., J.A.M., and S.S.W) was supported by the U.S. Department of Energy, Basic Energy Sciences, Materials Sciences and Engineering Division. Experiments were performed in part at the Center for Functional Nanomaterials located at Brookhaven National Laboratory, which is supported by the U.S. Department of Energy under contract number DE-AC02-98CH10886. Raman data were collected on an instrument obtained with an NSF-MRI grant OCE-1336724. We also acknowledge Dr. Dmytro Nykypanchuk at Brookhaven National Laboratory for help with lifetime measurements. NEXAFS measurements were collected at the U7A NIST/DOW beamline, located at the National Synchrotron Light Source (NSLS) at Brookhaven National Laboratory (BNL), which is supported by the U.S. Department of Energy under contract number DE-AC02-98CH10886.

## ■ REFERENCES

(1) Nikl, M.; Bohacek, P.; Mihokova, E.; Kobayashi, M.; Ishii, M.; Usuki, Y.; Babin, V.; Stolovich, A.; Zazubovich, S.; Bacci, M. *J. Lumin.* **2000**, *87*–*89*, 1136–1139.

(2) Errandonea, D.; Manjón, F. J. *Prog. Mater. Sci.* **2008**, *53*, 711–773.

(3) Errandonea, D.; Pellicer-Porres, J.; Manjón, F.; Segura, A.; Ferrer-Roca, C.; Kumar, R.; Tschauner, O.; Rodríguez-Hernández, P.; López-Solano, J.; Radescu, S. *Phys. Rev. B* **2005**, *72*, 174106.

(4) Treadaway, M. J.; Powell, R. C. *J. Chem. Phys.* **1974**, *61*, 4003–4011.

(5) Grasser, R.; Scharmann, A.; Strack, K.-R. *J. Lumin.* **1982**, *27*, 263–272.

(6) Zhang, Y.; Holzwarth, N.; Williams, R. *Phys. Rev. B* **1998**, *57*, 12738.

(7) Mikhailik, V.; Kraus, H.; Miller, G.; Mykhaylyk, M.; Wahl, D. *J. Appl. Phys.* **2005**, *97*, 083523.

(8) Su, Y.; Li, L.; Li, G. *Chem. Mater.* **2008**, *20*, 6060–6067.

(9) Meunier, P.; Bravin, M.; Bruckmayer, M.; Giordano, S.; Loidl, M.; Meier, O.; Pröbst, F.; Seidel, W.; Sisti, M.; Stodolsky, L. *Appl. Phys. Lett.* **1999**, *75*, 1335–1337.

(10) Errandonea, D.; Somayazulu, M.; Hausermann, D. *Phys. Status Solidi B* **2002**, *231*, R1–R3.

(11) Arora, S.; Chudasama, B. *Cryst. Res. Technol.* **2006**, *41*, 1089–1095.



DOI: 10.1021/cm503611q
*Chem. Mater.* 2015, 27, 778–792

(12) Mahootian, N.; Kikuchi, C.; Viehmann, W. *J. Chem. Phys.* **2003**, *48*, 1097−1102.
(13) Pang, M.; Lin, J.; Wang, S.; Yu, M.; Zhou, Y.; Han, X. *J. Phys.: Condens. Matter* **2003**, *15*, 5157.
(14) Wang, Y.; Ma, J.; Tao, J.; Zhu, X.; Zhou, J.; Zhao, Z.; Xie, L.; Tian, H. *Mater. Lett.* **2006**, *60*, 291−293.
(15) Sun, L.; Cao, M.; Wang, Y.; Sun, G.; Hu, C. *J. Cryst. Growth* **2006**, *289*, 231−235.
(16) Hou, Z.; Li, C.; Yang, J.; Lian, H.; Yang, P.; Chai, R.; Cheng, Z.; Lin, J. *J. Mater. Chem.* **2009**, *19*, 2737−2746.
(17) Ryu, J. H.; Yoon, J.-W.; Lim, C. S.; Oh, W.-C.; Shim, K. B. *Ceram. Int.* **2005**, *31*, 883−888.
(18) Mao, Y.; Zhang, F.; Wong, S. S. *Adv. Mater.* **2006**, *18*, 1895−1899.
(19) Zhou, H.; Wong, S. S. *ACS Nano* **2008**, *2*, 944−958.
(20) Mao, Y.; Wong, S. S. *J. Am. Chem. Soc.* **2004**, *126*, 15245−15252.
(21) Zhang, F.; Wong, S. S. *Chem. Mater.* **2009**, *21*, 4541−4554.
(22) Zhang, F.; Sfeir, M. Y.; Misewich, J. A.; Wong, S. S. *Chem. Mater.* **2008**, *20*, 5500−5512.
(23) Li, P.; Zhao, X.; Jia, C.-j.; Sun, H.; Sun, L.; Cheng, X.; Liu, L.; Fan, W. *J. Mater. Chem. A* **2013**, *1*, 3421−3429.
(24) Shang, M.; Wang, W.; Zhang, L.; Sun, S.; Wang, L.; Zhou, L. *J. Phys. Chem. C* **2009**, *113*, 14727−14731.
(25) Guo, Y.; Zhang, G.; Gan, H.; Zhang, Y. *Dalton Trans.* **2012**, *41*, 12697−12703.
(26) Lee, S. H.; Deshpande, R.; Parilla, P. A.; Jones, K. M.; To, B.; Mahan, A. H.; Dillon, A. C. *Adv. Mater.* **2006**, *18*, 763−766.
(27) Banerjee, S.; Wong, S. S. *Nano Lett.* **2002**, *2*, 195−200.
(28) Peng, X.; Chen, J.; Misewich, J. A.; Wong, S. S. *Chem. Soc. Rev.* **2009**, *38*, 1076−1098.
(29) Banerjee, S.; Wong, S. S. *J. Am. Chem. Soc.* **2003**, *125*, 10342−10350.
(30) Peng, X.; Sfeir, M. Y.; Zhang, F.; Misewich, J. A.; Wong, S. S. *J. Phys. Chem. C* **2010**, *114*, 8766−8773.
(31) Peng, X.; Misewich, J. A.; Wong, S. S.; Sfeir, M. Y. *Nano Lett.* **2011**, *11*, 4562−4568.
(32) Robel, I.; Kuno, M.; Kamat, P. V. *J. Am. Chem. Soc.* **2007**, *129*, 4136−4137.
(33) Li, G.-S.; Zhang, D.-Q.; Yu, J. C. *Environ. Sci. Technol.* **2009**, *43*, 7079−7085.
(34) Leschkies, K. S.; Divakar, R.; Basu, J.; Enache-Pommer, E.; Boercker, J. E.; Carter, C. B.; Kortshagen, U. R.; Norris, D. J.; Aydil, E. S. *Nano Lett.* **2007**, *7*, 1793−1798.
(35) Yan, C.; Dadvand, A.; Rosei, F.; Perepichka, D. F. *J. Am. Chem. Soc.* **2010**, *132*, 8868−8869.
(36) Zhu, Y.; Cui, S.; Chen, X.; Xu, W.; Zhou, P.; Wang, Y.; Xu, L.; Song, H.; Huang, L.; Huang, W. *Nanoscale* **2014**, *6*, 8075−8083.
(37) Kar, A.; Datta, A.; Patra, A. *J. Mater. Chem.* **2010**, *20*, 916−922.
(38) Blasse, G.; Grabmaier, B. C. *Luminescent Materials*; Springer: Berlin, 1994.
(39) Han, J.; Wang, L.; Wong, S. S. *J. Phys. Chem. C* **2014**, *118*, 5671−5682.
(40) Han, J.; Wang, L.; Wong, S. S. *RSC Adv.* **2014**, *4*, 34963−34980.
(41) Koroteev, V.; Bulusheva, L.; Asanov, I.; Shlyakhova, E.; Vyalikh, D.; Okotrub, A. *J. Phys. Chem. C* **2011**, *115*, 21199−21204.
(42) Liu, C.; Lee, S.; Su, D.; Zhang, Z.; Pfefferle, L.; Haller, G. L. *J. Phys. Chem. C* **2012**, *116*, 21742−21752.
(43) Zhou, J.; Fang, H.; Maley, J.; Ko, J.; Murphy, M.; Chu, Y.; Sammynaiken, R.; Sham, T. *J. Phys. Chem. C* **2009**, *113*, 6114−6117.
(44) Hamad, K.; Roth, R.; Rockenberger, J.; Van Buuren, T.; Alivisatos, A. *Phys. Rev. Lett.* **1999**, *83*, 3474.
(45) Lee, J. R.; Meulenberg, R. W.; Hanif, K. M.; Mattoussi, H.; Klepeis, J. E.; Terminello, L. J.; van Buuren, T. *Phys. Rev. Lett.* **2007**, *98*, 146803.
(46) Zhang, F.; Sfeir, M. Y.; Misewich, J. A.; Wong, S. S. *Chem. Mater.* **2008**, *20*, 5500−5512.
(47) Qu, L.; Peng, X. *J. Am. Chem. Soc.* **2002**, *124*, 2049−2055.
(48) Hines, D. A.; Kamat, P. V. *J. Phys. Chem. C* **2013**, *117*, 14418−14426.
(49) Pan, Z.; Zhao, K.; Wang, J.; Zhang, H.; Feng, Y.; Zhong, X. *ACS Nano* **2013**, *7*, 5215−5222.
(50) Gao, B.; Shen, C.; Zhang, B.; Zhang, M.; Yuan, S.; Yang, Y.; Chen, G. *J. Appl. Phys.* **2014**, *115*, 193104.
(51) Robel, I.; Subramanian, V.; Kuno, M.; Kamat, P. V. *J. Am. Chem. Soc.* **2006**, *128*, 2385−2393.
(52) Banerjee, S.; Hemraj-Benny, T.; Balasubramanian, M.; Fischer, D. A.; Misewich, J. A.; Wong, S. S. *Chem. Commun.* **2004**, 772−773.
(53) Banerjee, S.; Hemraj-Benny, T.; Balasubramanian, M.; Fischer, D. A.; Misewich, J. A.; Wong, S. S. *Chem. Phys. Chem.* **2004**, *5*, 1416−1422.
(54) Hemraj-Benny, T.; Banerjee, S.; Sambasivan, S.; Balasubramanian, M.; Fischer, D. A.; Eres, G.; Puretzky, A. A.; Geohegan, D. B.; Lowndes, D. H.; Han, W. *Small* **2006**, *2*, 26−35.
(55) Banerjee, S.; Hemraj-Benny, T.; Sambasivan, S.; Fischer, D. A.; Misewich, J. A.; Wong, S. S. *J. Phys. Chem. B* **2005**, *109*, 8489−8495.
(56) Lakowicz, J. R.; Geddes, C. D. *Topics in Fluorescence Spectroscopy*; Springer: Berlin, 1991; Vol. *1*.
(57) Page, A. G.; Godbole, S. V.; Sastry, M. D. *J. Phys. Chem. Solids.* **1989**, *50*, 571−575.
(58) Sleight, A. *Acta Crystallogr., Sect. B* **1972**, *28*, 2899−2902.
(59) Mancheva, M. N.; Iordanova, R. S.; Klissurski, D. G.; Tyuliev, G. T.; Kunev, B. N. *J. Phys. Chem. C* **2007**, *111*, 1101−1104.
(60) Nakamoto, K. *Infrared and Raman Spectra of Inorganic and Coordination Compounds*; Wiley Online Library: 1978.
(61) Basiev, T.; Sobol, A.; Voronko, Y. K.; Zverev, P. *Opt. Mater.* **2000**, *15*, 205−216.
(62) Porto, S.; Scott, J. *Phys. Rev.* **1967**, *157*, 716.
(63) Kaminskii, A. A.; Eichler, H. J.; Ueda, K.-i.; Klassen, N. V.; Redkin, B. S.; Li, L. E.; Findeisen, J.; Jaque, D.; Garcia-Sole, J.; Fernandez, J. *Appl. Opt.* **1999**, *38*, 4533−4547.
(64) Suda, J.; Sato, T. *J. Phys. Soc. Jpn.* **1997**, *66*, 1707−1713.
(65) Golubović, A.; Gajić, R.; Dohčević-Mitrović, Z.; Nikolić, S. *J. Alloys Compd.* **2006**, *415*, 16−22.
(66) Su, Y.; Li, G.; Xue, Y.; Li, L. *J. Phys. Chem. C* **2007**, *111*, 6684−6689.
(67) Mikhailik, V.; Kraus, H.; Wahl, D.; Itoh, M.; Koike, M.; Bailiff, I. *Phys. Rev. B* **2004**, *69*, 205110.
(68) Sokolenko, E. V.; Zhukovskii, V. M.; Buyanova, E. S.; Krasnobaev, Y. A. *Inorg. Mater.* **1998**, *34*, 499−502.
(69) Grasser, R.; Himam, M. I.; Scharmann, A.; Ströde, J. *Phys. Status Solidi A* **1992**, *130*, K225−K228.
(70) Campos, A. B.; Simões, A. Z.; Longo, E.; Varela, J. A.; Longo, V. M.; de Figueiredo, A. T.; De Vicente, F. S.; Hernandes, A. C. *Appl. Phys. Lett.* **2007**, *91*, 051923.
(71) Grasser, R.; Scharmann, A.; Strack, K. R. *J. Lumin.* **1982**, *27*, 263−272.
(72) Liu, T.; Chen, J.; Yan, F. *J. Lumin.* **2009**, *129*, 101−104.
(73) Ryu, J. H.; Park, G. S.; Kim, K. M.; Lim, C. S.; Yoon, J.-W.; Shim, K. B. *Appl. Phys. A: Mater. Sci. Process.* **2007**, *88*, 731−736.
(74) Chen, S.-J.; Li, J.; Chen, X.-T.; Hong, J.-M.; Xue, Z.; You, X.-Z. *J. Cryst. Growth* **2003**, *253*, 361−365.
(75) Han, J. K.; Hannah, M. E.; Piquette, A.; Talbot, J. B.; Mishra, K. C.; McKittrick, J. *ECS J. Solid State Sci. Technol.* **2012**, *1*, R98−R102.
(76) Jung, K. Y.; Lee, C. H.; Kang, Y. C. *Mater. Lett.* **2005**, *59*, 2451−2456.
(77) Schaller, R. D.; Sykora, M.; Pietryga, J. M.; Klimov, V. I. *Nano Lett.* **2006**, *6*, 424−429.
(78) Kamat, P. V. *J. Phys. Chem. C* **2008**, *112*, 18737−18753.
(79) Hillhouse, H. W.; Beard, M. C. *Curr. Opin. Colloid Interface Sci.* **2009**, *14*, 245−259.
(80) van Sark, W. G. J. H. M.; Frederix, P. L. T. M.; Van den Heuvel, D. J.; Gerritsen, H. C.; Bol, A. A.; van Lingen, J. N. J.; de Mello Donegá, C.; Meijerink, A. *J. Phys. Chem. B* **2001**, *105*, 8281−8284.
(81) Tvrdy, K.; Kamat, P. V. *J. Phys. Chem. A* **2009**, *113*, 3765−3772.
(82) Stodilka, R. Z.; Carson, J. J. L.; Yu, K.; Zaman, M. B.; Li, C.; Wilkinson, D. *J. Phys. Chem. C* **2009**, *113*, 2580−2585.


DOI: 10.1021/cm503611q
*Chem. Mater.* 2015, 27, 778−792

(83) Longo, V. M.; Gracia, L.; Stroppa, D. G.; Cavalcante, L. S.; Orlandi, M.; Ramirez, A. J.; Leite, E. R.; Andrés, J.; Beltrán, A.; Varela, J. A.; Longo, E. *J. Phys. Chem. C* **2011**, *115*, 20113−20119.
(84) Völker, J.; Zhou, X.; Ma, X.; Flessau, S.; Lin, H.; Schmittel, M.; Mews, A. *Angew. Chem., Int. Ed.* **2010**, *49*, 6865−6868.
(85) Kucheyev, S. O.; Baumann, T. F.; Sterne, P. A.; Wang, Y. M.; van Buuren, T.; Hamza, A. V.; Terminello, L. J.; Willey, T. M. *Phys. Rev. B* **2005**, *72*, 035404.
(86) Zhou, J. G.; Fang, H. T.; Hu, Y. F.; Sham, T. K.; Wu, C. X.; Liu, M.; Li, F. *J. Phys. Chem. C* **2009**, *113*, 10747−10750.
(87) Zhou, J. G.; Fang, H. T.; Maley, J. M.; Ko, J. Y. P.; Murphy, M.; Chu, Y.; Sammynaiken, R.; Sham, T. K. *J. Phys. Chem. C* **2009**, *113*, 6114−6117.
(88) Annese, E.; Fujii, J.; Vobornik, I.; Rossi, G. *J. Phys. Chem. C* **2011**, *115*, 17409−17416.
(89) Petraki, F.; Peisert, H.; Biswas, I.; Chassé, T. *J. Phys. Chem. C* **2010**, *114*, 17638−17643.
(90) Mikhailik, V.; Kraus, H.; Wahl, D.; Itoh, M.; Koike, M.; Bailiff, I. *Phys. Rev. B* **2004**, *69*, 205110.
(91) Ingham, B.; Hendy, S.; Chong, S.; Tallon, J. *Phys. Rev. B* **2005**, *72*, 075109.
(92) Ruiz-Fuertes, J.; Errandonea, D.; Segura, A.; Manjón, F.; Zhu, Z.; Tu, C. *High Pressure Res.* **2008**, *28*, 565−570.



DOI: 10.1021/cm503611q
*Chem. Mater.* 2015, 27, 778−792